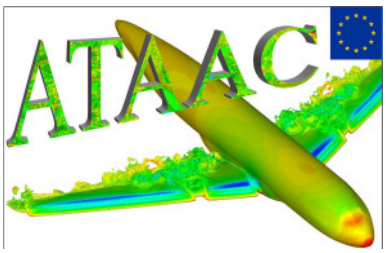

Deliverable D3.2-36

Extended excerpt related to the test case: "Flow over a periodical arrangement of 2D hills"

Final report on "Assessment of the RSM, URANS and hybrid models with respect to the different roadmaps including the industrial application challenges"

June 2012

S. Jakirlic, TU Darmstadt

Table of Contents

1 Summary of extended excerpt

This is an extended excerpt from the ATAAC project deliverable D3.2-36 dealing with the computational activity related to the test case "**Flow over a periodical arrangement of 2D hills**", denoted presently by ST01 - "Stepping Stone 01".

1.1 ST01: 2D periodic hill (TUD)

The flow over a series (in a periodic sense) of smoothly contoured symmetric hills (Figure 1) has numerous interesting features: streamwise periodicity, separation from a continuous curved surface, reattachment, flow relaxation in the post-reattachment region, alternating adverse (flow deceleration) and favourable (flow acceleration) pressure gradient effects (globally along the flow but even across the same streamwise location - e.g. at the windward side, Figure 1 right), streamline curvature effects, wall proximity effects, Reynolds-stress anisotropy, etc. The flow configurations characterized by Reynolds numbers based on the hill height and mean velocity at the hill crest of Re_H=10600 and Re_H=37000 were in focus of the computational activities in the framework of the ATAAC project.

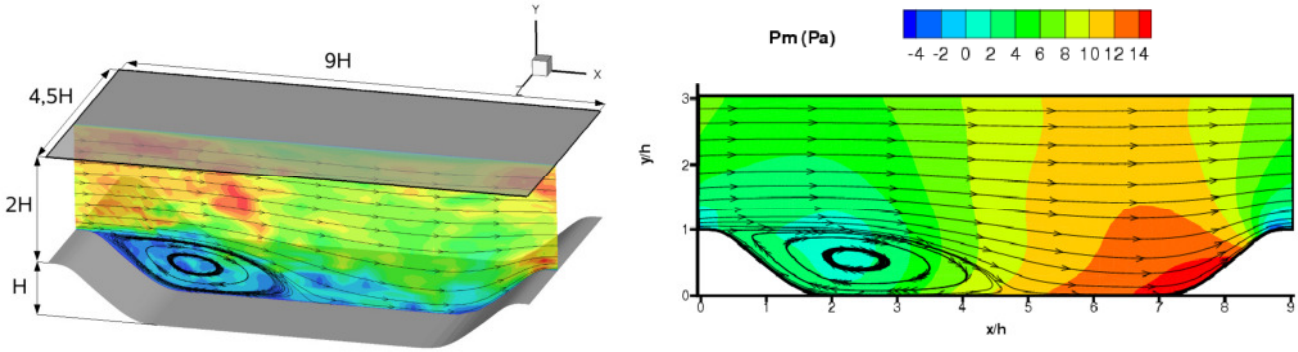

Figure 1: Periodic flow over a 2-D hill: flow domain considered and its dimensions. The instantaneous velocity field (left) and time-averaged pressure field (right) are obtained by a zonal hybrid LES/RANS model, Jakirlic et al. (2011). The results relate to the lower Reynolds number case, Re_H=10600

1.1.1. Reference database

Detailed reference databases were made available by three highly-resolved Large-eddy Simulations (LES) - Mellen et al. (2000, LES-FMR), Temmerman and Leschziner (2001, LES-TL) (both result sets are summarized and analyzed in detail in Froehlich et al., 2005) and Breuer (2005, LES-B; see also Breuer et al., 2009). This configuration served as the test case of two ERCOFTAC SIG15 Workshops on refined turbulence modelling (Jakirlic et al., 2002; Manceau, 2003). Different RANS models ranging from simple 1-equation models (e.g. Spalart-Allmaras, 1994) via the 2-equation linear and non-linear eddy-viscosity-based model schemes up to differential second-moment closure models were applied. A very extensive analysis of the model performances is provided by Leschziner (2002). The present report is drawn upon this document to some extent. According to Leschziner the computational data exhibit high quality and reliability level. Accuracy and resolution checks were performed by analysing the spectra and two-point correlations at different location in the flow field, ratio of the representative grid spacing to the Kolmogorov scale, the contribution of the SGS (subgrid-scale) transport, etc. Recently, the above-mentioned computational database was enriched by a complementary experimental investigation performed by Rapp and Manhart (2007, EXP-RM; see also Rapp, 2008, Breuer et al., 2009 and Rapp and Manhart, 2011). In addition, the same flow geometry at two higher Reynolds numbers (Re_H=19000 and 37000) was also measured. The higher flow Reynolds number represents also the ATAAC test case.

Direct comparison of the four result sets for the lower Reynolds number flow reveals some mutual deviations, see Table 1 and Figure 2.

Re_H=10600	LES-B	LES-TL	LES-FMR	EXP-RM
$(x/H)_{SP}$	0.19	0.22	0.20	?
$(x/H)_{RP}$	4.69	4.72	4.56	4.24

Table 1: Locations of the separation $(x/H)_{SP}$ and reattachment $(x/H)_{RP}$ points obtained by LES Simulations; LES-B (B - Breuer), LES-TL (TL – Temmerman, Leschziner) and LES-FMR (FMR – Fröhlich, Mellen, Rodi)

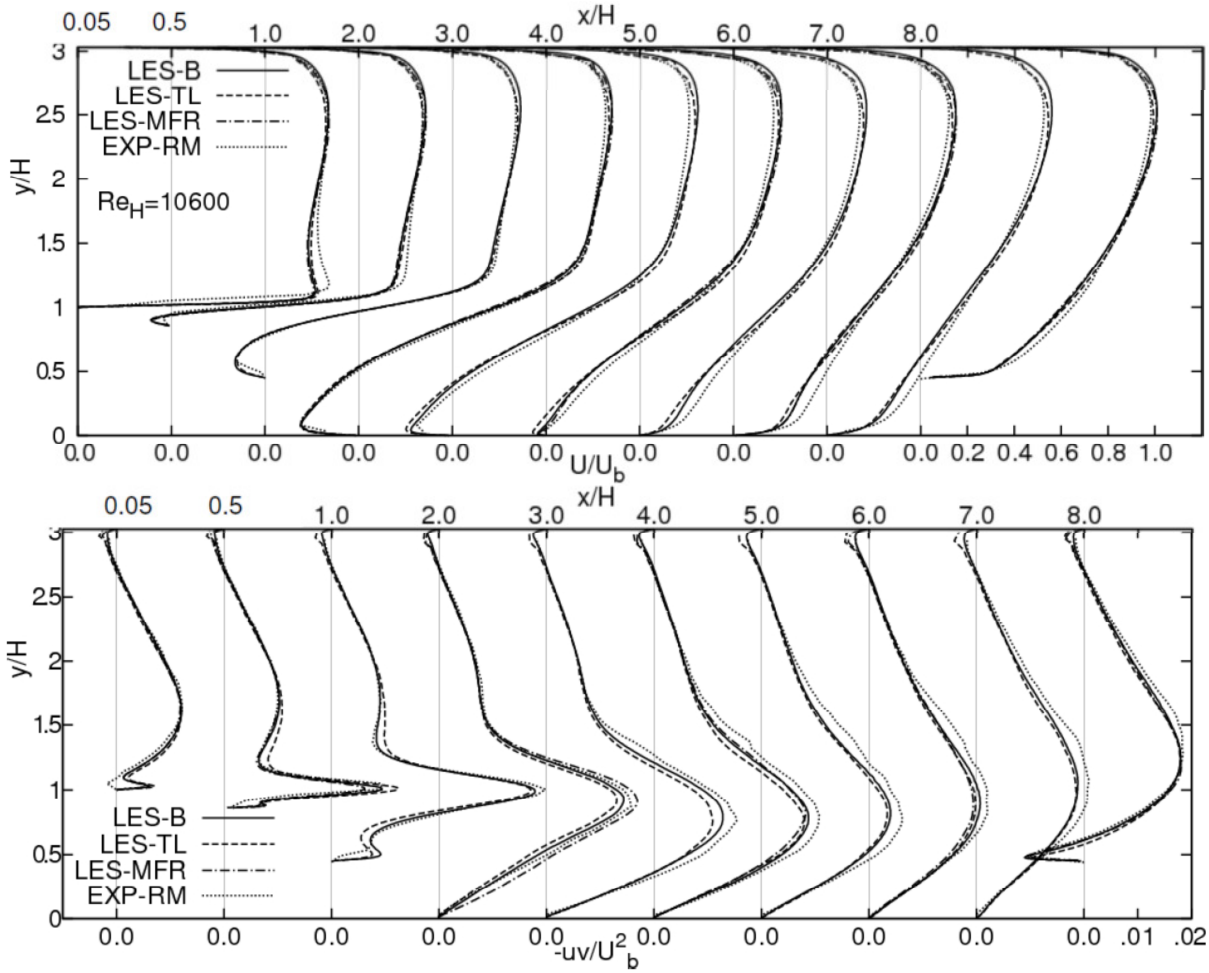

Figure 2: Evolution of the mean axial velocity and shear stress component profiles (Re_H=10600); EXP-RM (RM – Rapp, Manhart). See Table 1 for caption.

One notes slight differences. Especially visible is the departure of the experimental results from the LES database in the region of the hill crest (*x/H=0.05* and *0.5*) and post-reattachment recovery (*x/H=5, 6* and *7*) manifested through a more intensive flow acceleration. Furthermore the experimental results exhibit a somewhat higher shear stress component level in the recovery region. These departures are regarded to the largest extent as "irrelevant" for the model validation purposes. Finally, the LES database by Breuer (2005, approx. 13 Mio. grid points in total – upper wall was also resolved – are employed versus approx. 5 Mio. grid points in the Fröhlich et al., 2005, simulations) is adopted to be the reference one.

Figure 3 displays the comparison of the experimentally obtained results (axial velocity and shear stress components) for both Reynolds numbers considered. Figure 3 reveals the most pronounced Reynolds number dependent features of the averaged velocity and turbulence field One notes an appropriate shortening of the recirculation zone in terms of the Reynolds number – from *x/H=4.21* to *x/H=3.76* - due to turbulence increase in the separated shear layer (important: profiles are normalized by the corresponding bulk velocity at the hill crest, which is about 3.5 times higher in the case of Re_H=37000). Important characteristics are a strongly emphasized velocity overshoot at the hill crest corresponding to more intensive acceleration as well as the position of the shear stress maxima which is appropriately shifted towards the wall.

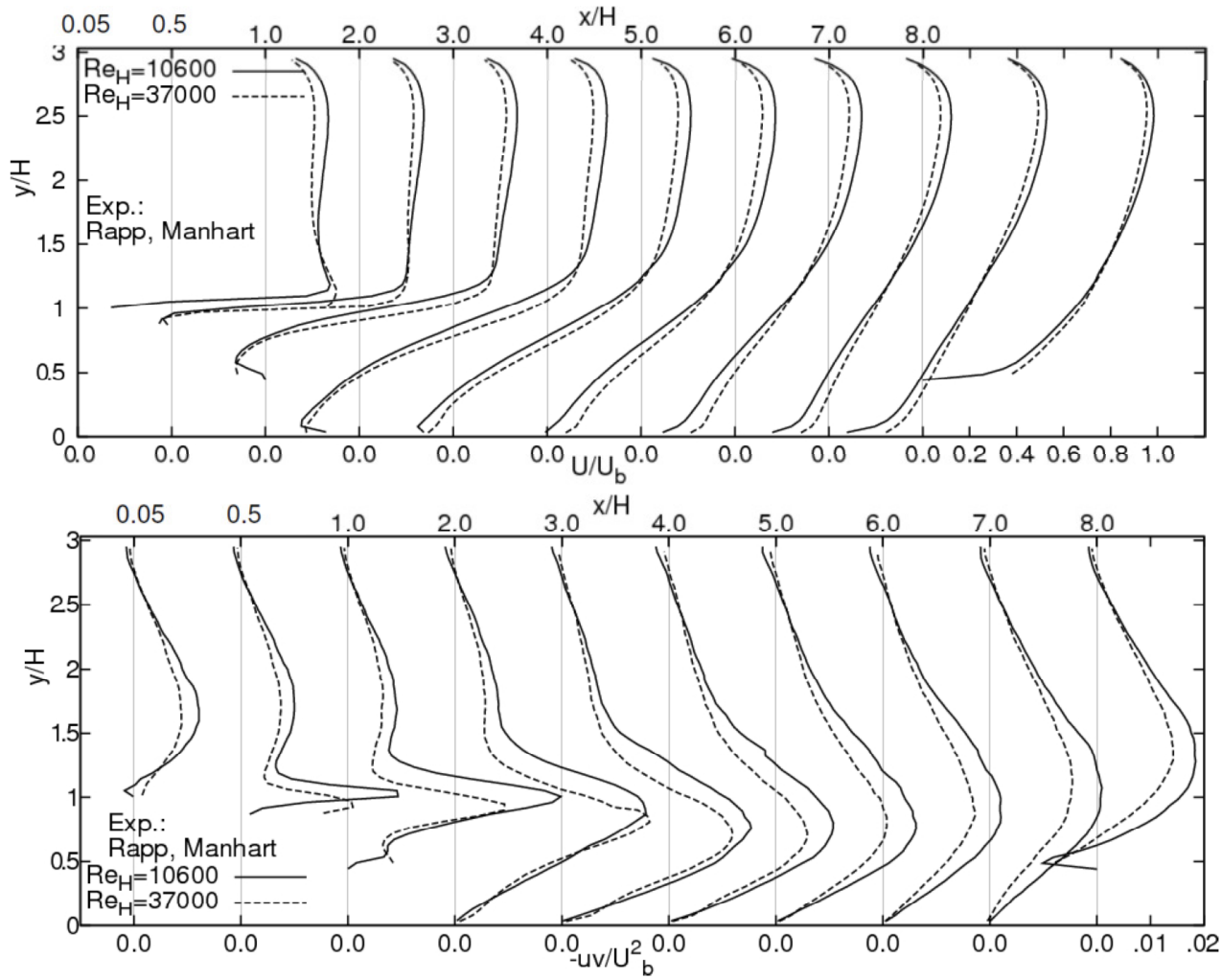

Figure 3: Evolution of the mean axial velocity and shear stress component profiles obtained experimentally at two flow Reynolds numbers Re_H=10600 and Re_H=37000, Rapp (2008) and Rapp and Manhart (2011)

1.1.2. Contributors and turbulence models employed

Following ten groups contributed to the collaborative computation of this test case: CHA (Chalmers University Gothenburg), FOI (Swedish Defence Research Agency), ICL (Imperial College London), NTS (New Technologies and Services, St. Petersburg), TUB (Technical University Berlin), TUD (Technische Universität Darmstadt), UniMAN (University of Manchester), IMFT (Institut de Mécanique des Fluides de Toulouse), NUM (NUMECA - Numerical Mechanics Application International, Brussels) and ANS (ANSYS

Germany). Four (i.e. three) groups of cross-plotted results (corresponding to both Reynolds numbers respectively) are presented in accordance with the model formulations employed:

I. RANS, Eddy-viscosity model (EVM) group: 1-eq. model due to Spalart-Allmaras (SA, 1994), two-equation models (k-ε, Launder and Sharma, 1994, and k-ω SST, Menter, 1994) and 4-equation ERM-based models (ERM - Elliptic Relaxation Method, see e.g. Laurence et al., 2004)
II. RANS, Reynolds stress models (RSM): Differential (DRSM) and Explicit Algebraic (EARSM) model variants coupled with both ε-equation and ω-equation (Shima, 1993; Speziale et al. - SSG, 1991; Jakirlic and Hanjalic, 2002; Manceau and Hanjalic, 2002; Wallin and Johansson, 2000, Menter et al., 2009)
III. DES (Detached-Eddy Simulation) related models: DES, Delayed DES (DDES) and Improved Delayed DES (IDDES), see e.g. Spalart (2001, 2009), both in conjunction with SA and k-ω SST. Also the DES method denoted as kDES based on a 1-equation model solving the transport equation for the kinetic energy of turbulence (applied by FOI, see Peng and Leicher, 2008)
IV. Unsteady simulations by PANS-k-ε (CHA; a seamless, so-called Partialy-Averaged Navier-Stokes method in conjunction with a low Reynolds number k-ε model, Ma et al., 2011), SAS-SST (SAS: Scale-Adaptive Simulation; this is the original version developed and applied by ANSYS, Menter et al., 2003; Menter and Egorov, 2010), SAS-DRSM (TUD; SAS methodology in conjunction with a differential low Reynolds number second-moment closure model, Maduta and Jakirlic, 2011), and two further seamless Hybrid RANS/LES models – one based on 0-Eq. RANS model (FOI, denoted by HYB0; also a HYB0 modification accounting for the energy back-scatter – denoted by HYB0M – was tested, see Peng, 2005 and 2006) and another on the ERM-like (ERM – Elliptic Relaxation Model) phi-f model (UniMan; the results of the RANS calculations using the same model are displayed within the first group, Billard et al., 2010, Jarrin et al., 2009 and Uribe et al., 2010).

Mandatory mesh consisting of $N_x x N_y x N_z = 160x160x60$ grid cells was designed by an appropriate coarsening of the 13 M cells fine grid made available by Breuer (2005), Figure 4. This grid was appropriate to be applied for computing the flows at both Reynolds numbers considered (Figure 5 illustrates the distribution of the non-dimensional distance y^+ of the wall-next numerical node along the lower wall extracted from the velocity fields obtained by the SAS-DRSM model; accordingly the grid is sufficiently fine also for the higher Reynolds number case; the NTS group refined further this grid for the Re_H=37000 case consisting finally of 180 grid cells in the normal direction). The grid exhibits a high level of orthogonality. It should be noted that not all computational groups used the proposed grid, see model and grid details in the tables specifying the participating groups.

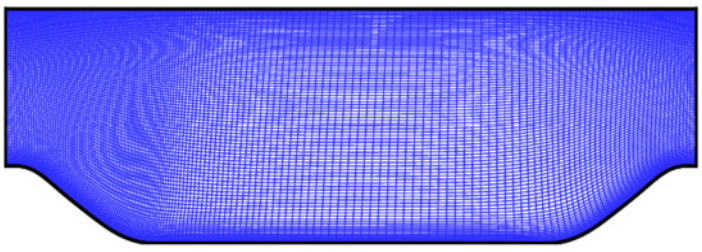

Figure 4: Computational grid

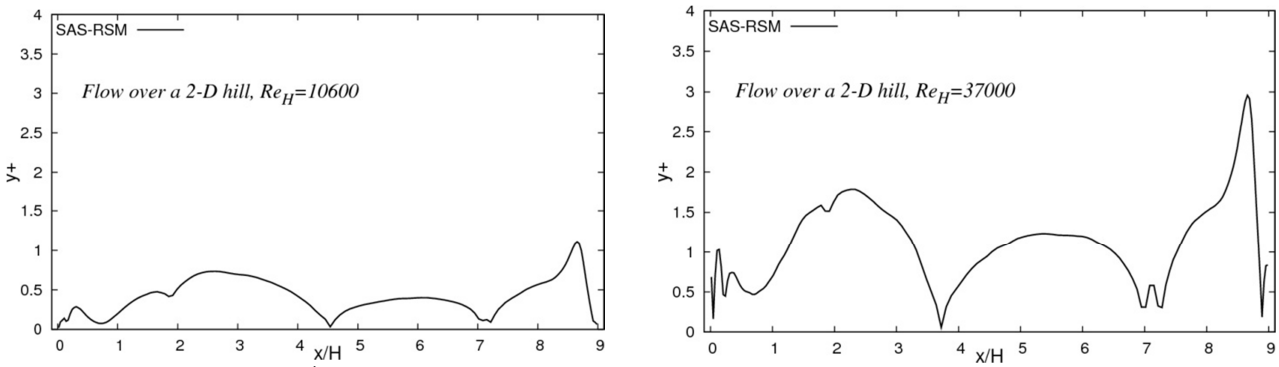

Figure 5: y^+ distribution at the lower wall for both Reynolds numbers considered

Moreover, the ICL group applied the three-2dhill-segment geometry by specifying the LES data at the inlet and zero-gradient conditions at the outlet, Figure 6. The motivation for such an application was the elimination of a possibly negative influence of the streamwise periodicity on the model performances, because the errors in the solution in the inner flow domain can be fed back through the inlet plane, thus amplifying the departure of the "real" model solution, Leschziner (2002).

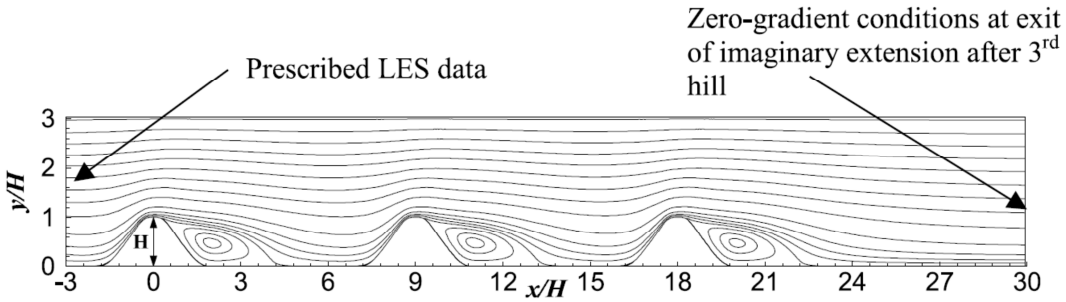

Figure 6: Three-2dhill-segment geometry and corresponding boundary conditions, Leschziner (2002)

1.1.3. Overall flow features

Here, the basic features of the turbulent flow separation pertinent to the presently considered configuration are recalled before starting with the result presentation and corresponding discussion. Their qualitative behaviour is similar in both Reynolds number cases. The flow over a symmetric 2D hill is characterized by a nominally two-dimensional separation pattern and is steady in mean. However, the highly-unsteady shear layer that "separates" the main stream (through-flow) from the recirculation is dominated by the organized, large-scale coherent structures, influencing to a large extent the overall flow behaviour. It should be recalled that the conventional, time-averaged RANS methods, almost independent of the modelling level, unlike in some flows separated from the sharp-edged surfaces (with fixed separation point; e.g., backward-facing step geometries), perform fairly poor in the flows separated from continuous surfaces (it is also valid for flows separated from fences and ribs). The latter flow configurations exhibit a number of features typically associated with an unsteady flow separation (highly intermittent separation and reattachment regions). Here, the separation point oscillates over a larger portion of the wall. These oscillations are conveyed into the separated shear layer, whose spreading is much more intensive. Likewise, the mean dividing streamline is much more complex (stronger curvature and more intensive turbulence production). All these features can neither qualitatively nor quantitatively be reproduced by a RANS model. The outcome is a fairly poor reproduction of turbulence field pertinent to a low turbulence activity in the separated shear layer and, consequently, the mean velocity field characterized by a much longer recirculation zone.

1.1.4. Results and discussion

The results presentation includes the friction factor development at the lower wall, streamline patterns (and consequently the locations of the separation and reattachment points) and the profiles of mean axial velocity, turbulent kinetic energy and shear stress component at four selected streamwise locations: *x/H=0.05*, *2.0*, *6.0* and *8.0*. The flow at these locations, chosen in accordance with the analysis of Leschziner (2002), is characterized as follows

- *x/H=0.05* – this location corresponds to the narrowest cross-section where the most intensive acceleration occurs, not only globally but also locally (see negative pressure in Figure 1-right and velocity profile overshoot, Figure 2-upper). The influence of the curved wall boundary layer (longitudinal curvature) upstream of the hill (windward side) on the flow parameter at this location is large. The flow acceleration causes an appropriate attenuation of turbulence (stabilizing curvature) followed by enhanced turbulence production due to highly time- and space-dependent intermittent separation occurring over a larger surface on the leeward side of the hill, see strong jump in the turbulence level in the region of the separated shear layer after this position, Figure 2-lower.
- *x/H=2.0* – this location crosses the recirculation zone and the curved detached shear layer featured by intensive mixing and an additional turbulence production due to the (local) streamline-curvature-induced strain rate (stabilizing curvature). Keeping in mind that this shear layer impinges at the reattachment region (shear layer – wall interaction: strong modification of the fluctuating pressure field causing intensive turbulent energy redistribution among stress components and consequently strong modulation of the Reynolds stress anisotropy) followed by the flow bifurcation it becomes clear how important is its correct capturing.
- *x/H=6.0* – position in the post-reattachment recovery region: due to a short distance between the reattachment region (x/H=4.7 for Re_H=10600 and x/H=3.76 for Re_H=37000) and the windward hill side there is a partial flow recovery. Both viscous effects (development of a new boundary layer after reattachment) and non-viscous interaction between the outer layer and wall are important
- *x/H=8.0* – position at the windward side of the hill where the mean flow is strongly re-accelerated. On the other hand, the flow is locally (region around the foot of the hill - here, even a small separation bubble appears) decelerated (see pressure increase in Figure 1-right)

All these features should be correctly represented by a turbulence model. It should be recalled that the computational activity within the ATAAC project is primarily directed towards the employment of the turbulence models on the second-moment closure level (algebraic and differential Reynolds stress models).

The performances of the models will be discussed in parallel with respect to both Reynolds numbers. The profiles of all quantities exhibit qualitatively very similar shape in the Reynolds number range considered. Accordingly, the results analysis can be conducted jointly for both Reynolds numbers. The model performances concerning the Reynolds number dependence on the flow development differ primarily with respect to the turbulence enhancement in the separated shear layer and the consequent separation bubble shortening.

1.1.4.1 EVM RANS models

In spite of the latter objective, a reasonable number of contributions using different eddy-viscosity models were submitted. As the results obtained are comparable to those pertinent to the Reynolds stress models a selection of them will be displayed (Figure 8-Figure 10) and discussed without performing an in-dept analysis. The results obtained confirmed the findings of both SIG15 workshops discussed by Leschziner (2002):

- The basic flow topology was returned by all EVM models applied. However, apart of the overall velocity profile evolution obtained by the "simplest" linear k-ε model due to Launder and Sharma (Figure 9; employed by the ICL group), all other results agree poorly with the reference database.
- The k-ω SST model (employed by the NTS Group) predicts the separation region being too large compared to the reference database. Similar result was obtained by the 1-equation SA model. The turbulence level in the separated shear layer (*x/H=2*) is by far too low. It is well-known that the turbulence level in the separated shear layer controls the size of the recirculation zone. For example, a higher level of the shear stress implies an enhancement of the fluid entrainment into the shear layer - higher momentum transport - and consequently a shorter recirculation bubble. Contrary to that, a lower turbulence level is consistent with a longer separation zone. Presently, the shear stress level is very low having an excessive separation as a consequence, the fact being in line with the previous statement. On the other hand, the linear EVM models (the Launder and Sharma model and two UniMAN models based on the Elliptic-Relaxation Method - ERM) – employed in conjunction with the dissipation rate ε as the scale-supplying variable - predict much shorter recirculation zones despite the turbulence level being comparably low with the one obtained by the k-ω SST and SA models.
- Correct capturing of the wall-proximity effects is one of the important prerequisite for the successful computation of the present case. Accordingly, two ERM-based models were employed by the UniMAN group. These models account, to a certain extent, for the near-wall anisotropy through the inclusion of the normal-to-wall stress component into definition of the turbulent viscosity damping by approaching the solid wall. It led to a very good prediction of the reattachment length (despite delayed separation), see friction factor development obtained by the UniMAN-EVM-PhiBar model (dotted line in Figure 8). Unfortunately, all other results do not indicate any important improvement compared to the basic models. It should be recalled that the ERM EVM models reduces to the standard linear k-ε model apart of the near-wall region. The specification of both EVM-ERM models version could be found in Billard et al. (2010), see also Uribe et al. (2010).

1.1.4.2. RSM RANS models

The Reynolds stress models are inherently capable of capturing the majority of the time-averaged flow features and associated turbulence phenomena: streamline curvature effects, alternating deceleration and acceleration characterized by enhanced irrotational straining, pressure-scrambling process and Reynolds stress anisotropy. The 2-D hill case belongs to the category of the flows influenced locally by the streamline curvature, which in fact implies additional effects on the kinetic energy production rate through an extra strain rate $(U^2/R)\mathbf{n}_\sigma$, where U stands for the velocity component tangentially directed to the streamline - U_t, $\mathbf{n}_\sigma = R\, dt/d\sigma$ denotes direction normal to $\mathbf{t}$ and R is the radius of the streamline curvature. The global effect in the present case is the attenuation of the turbulence production in accordance with the mean flow angular momentum increase with curvature radius (stabilizing curvature). Contrary to the EVM models being beyond the reach of these effects, the RSM models accounts correctly for the turbulence level reduction. However, it led presently to a further weakening of the already low turbulence level (Figure 13 and Figure 22) and to a very long recirculation zone (see Figure 11-Figure 12 and Figure 20-Figure 21). This is in particular the case with the differential Reynolds stress models coupled with the ε-equation. Better overall agreement (turbulence level enhancement) was obtained by RSM models solving the ω-equation for the length-scale determination. This is especially the case when employing the Explicit Algebraic Reynolds Stress Models (FOI results in Figure 11-Figure 13 and Figure 20-Figure 22). On the other hand, the same models (e.g., FOI-EARSM-HWJ and FOI-DRSM) show less sensitivity to the Reynolds number increase concerning the recirculation zone shortening. Even opposite outcome – longer recirculation zone – was obtained.

Important improvement was obtained after introducing the SAS term into the JH DRSM (Jakirlic and Hanjalic, 2002) model (being already used in the framework of SAS-DRSM model; this term has the same functional dependency as the original formulation by Menter et al. – proposed in conjunction with the k-ω

SST model – the appropriately transformed model coefficients were slightly adjusted to the background RSM model). Let us recall that the introduction of the SAS-term in the instability sensitive second-moment closure version – unsteady flow simulation (denoted by SAS-DRSM, see next section) – contributed strongly to the turbulence enhancement (originating from the resolved motion) in the region around the separation point. The positive production of the ω- i.e. ε-variable affected by the SAS term led to the modelled turbulence suppression allowing development of the resolved motion. In a pure RANS model applied in the steady computational mode an opposite action is necessary: the scale-supplying variable has to be appropriately reduced leading consequently to the increase of the (modelled) turbulence. Accordingly, the same SAS-term was introduced into the ω_h-equation but with the negative sign. The evaluation of the term has shown that it was active only in the separation region, Figure 7. The inclusion of this term led to appropriate increase of the turbulence activity in the region aligned with the mean dividing streamline resulting in the improved capturing of the velocity field and recirculation zone shortening (see Figure 11-Figure 13 and Figure 20-Figure 22), Maduta and Jakirlic (2011).

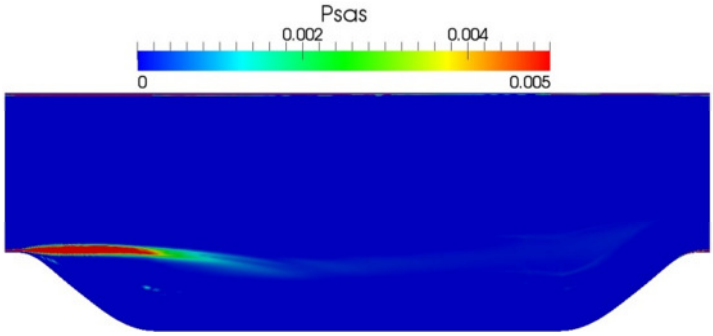

Figure 7: Magnitude of the "negative" P_{SAS} term in the 2D hill flow field introduced into the JH RSM model

It should also be noted that the application of all RANS models resulted in the steady solution. The so-called "temporal under-relaxation" was applied sometimes to strengthen the diagonal dominance of the coefficient matrix, implying that actually unsteady computations were performed. However, such an unsteady calculation ended up, as expected, in a steady solution.

1.1.4.3. Unsteady flow simulations: DES-, Seamless hybrid RANS/LES (PANS, HYB0 and HRLV2F) and SAS-related models

Here, different, LES-related unsteady simulations using appropriate models were performed. The simulations were performed employing four DES-relevant schemes (DES, Delayed DES – DDES, Improved DDES – IDDES and kDES, S.-H. Peng), three seamless hybrid RANS/LES / instability-sensitive Unsteady RANS model formulations - the PANS-k-ε formulation of Ma et al. (2010; CHA), a hybrid method based on an appropriate length scale switch enabling smooth transition between the RANS and LES sub-regions (S.-H. Peng, 2005, denoted by HYB0 relying on a 0-eq., mixing-length-type model), a hybrid model based on the v2f-type model (Uribe et al., 2010; denoted by HRLV2F) - and two novel instability-sensitive URANS models, denoted by SAS-SST (original SAS- based k-ω SST model proposed by Menter et al., 2010, ANS) and SAS-DRSM, of Maduta and Jakirlic (2011, TUD). The common feature of all these models is an appropriate modification of the scale-determining equation providing a dissipation rate level which suppresses the turbulence intensity towards the subgrid (i.e. subscale/subfilter) level in the regions where large coherent structures with a broader spectrum dominate the flow, allowing in such a way evolution of structural features of the associated turbulence. Whereas an appropriate dissipation level enhancement in the PANS method is achieved by reducing selectively (e.g. in the separated shear layer region) the destruction term in the model dissipation equation (i.e. its coefficient; the standard value $C_{\varepsilon,2}$= 1.92, prevailing in the near-wall region, decreases towards the value around 1.4 in the separated shear layer of the periodic 2D hill

flow), an additional production term was introduced into the ω equation in the SAS framework. This term is modelled in terms of the von Karman length scale comprising the second derivative of the velocity field, which is capable of capturing the vortex size variability, Menter et al. (2003, 2010). Whereas FOI employed the basic DES-SA model formulation, the NTS employed DDES and IDDES in conjunction with both k-ω SST and SA models using mandatory grid and TUB performed three simulations by the IDDES-SA model combination, but varying the grid size, grid structure (grid refined appropriately towards the walls and equidistant grid) and temporal resolution. Apart of the results obtained by the TUB-IDDES-SA3, employing more than 20 times coarser time step compared to the TUB-IDDES-SA1 and TUB-IDDES-SA2 simulations – leading to a higher turbulence level, all other results (apart of some slight differences) agree very well with the reference database in all characteristic regions of the flow. The SAS-SST and SAS-DRSM models exhibit high level of agreement with respect to all analyzed flow features (evolution of mean flow and turbulence quantities, friction factor development, size and shape of the recirculation zone) for both Reynolds numbers. The results obtained by the kDES model as well as two seamless hybrid schemes – HYB0 and HRLV2F – show important improvement compared to the background turbulence models they are based upon. However, some further refinement of the kDES and HYB0 schemes is necessary in order to get consistently good agreement in the entire flow domain. It is especially related to the specific intensification of the turbulence production in the region corresponding to the flow re-acceleration – streamwise position x/L=8, Figure 16 and Figure 19. On the other hand the mean velocity field exhibits high level agreement with the reference results indicating that the afore-mentioned departure could also be an outcome of the evaluating (averaging) procedure. The circumstances should be clarified.

1.1.5. Conclusions

It can be concluded without going into great details that the correct capturing of the present 2d-hill flow configuration is beyond the reach of the conventional, inherently steady RANS closures, almost independent of the modelling level. Some models perform better with respect to the global development of the mean velocity profile (e.g, the EARSM model coupled with Menter's ω-equation – also, the turbulence level obtained by this model at some positions agrees reasonably with the reference data). All other RANS results exhibit very poor agreement: skin friction development, shape, form and size of the separation bubble, profile shapes of turbulent quantities - qualitatively and quantitatively, including also their behaviour in the immediate wall vicinity, etc. Work on the possible improvement should include term-by-term modelling of the turbulent interactions (stress redistribution, turbulent diffusion, stress dissipation,…) in the budgets of the corresponding transport equations (governing the Reynolds stress components but also the scale-determining variables).

The inclusion of the negative SAS term – promoting the turbulence activity enhancement in the separated shear layer – fulfilled the expectations: the resulting mean flow variables (mean velocities and Reynolds stress components) displayed a very good agreement with respect to the reattachment length, profile shapes of both velocity and turbulence intensities – e.g. velocity overshoot due to acceleration on the hill crest, turbulence level in the separated shear layer - in the entire flow domain. Obviously that the structure of the model was "correct enough", the only weakness was inappropriate dissipation level. The effect of the negative SAS term was also checked in the "stable" flows, like e.g. in a channel flow. Here, there were no differences between the results obtained with the RANS-RSM-P_{SAS} and RANS-RSM models.

On the other hand, the results of the unsteady flow simulations (apart of both kDES and HYB0 models exhibiting some specific deviations of turbulence quantities from the reference results in the region of flow re-acceleration, see corresponding discussion), almost independently of the method used, follow closely the reference data in all characteristic flow regions: separation region, recirculation zone, reattachment, recovery region, windward hill region characterized by high re-acceleration of the flow and near-wall regions.

Identifier	Partner	Model
ICL-EVM-KEPS	ICL (Leschziner, Bentaleb)	Launder-Sharma near-wall k-ε model, 2D: 221x101 nodes
NTS-RANS-SST	NTS (Strelets, Adamian)	Menter's k-ω SST near-wall model, 2D: 161x161
NTS-RANS-SA	NTS (Strelets, Adamian)	Spalart-Allmaras near-wall model, 2D: 161x161
UniMAN-EVM-PhiAlpha	UniMAN (Billard, Laurence, Uribe)	ERM-PhiAlpha, 2D: 120x172
UniMAN-EVM-PhiFbar	UniMAN (Billard, Laurence, Uribe)	ERM-PhiFbar, 2D: 120x172

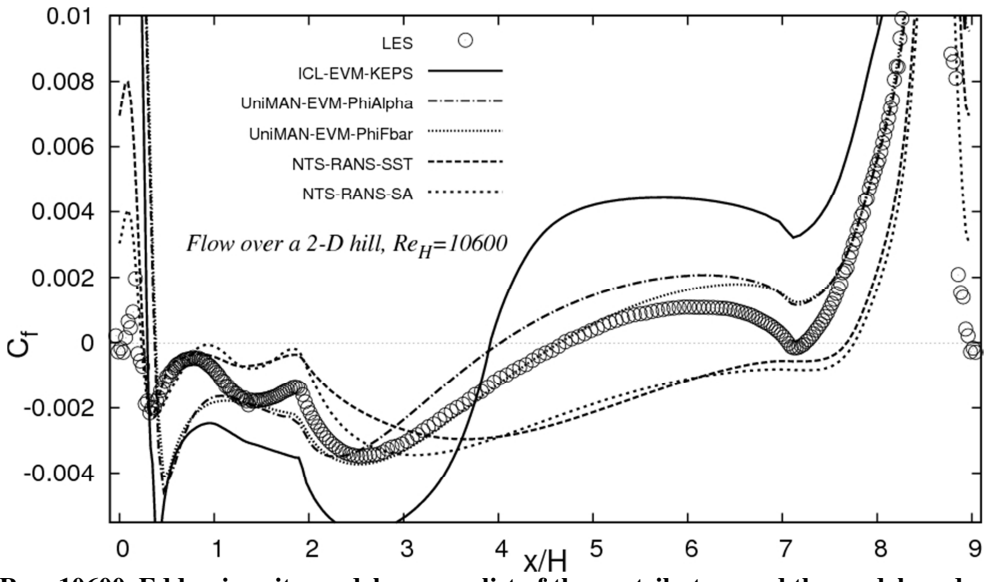

Figure 8: Re_H=10600, Eddy-viscosity model group – list of the contributors and the model used and friction factor

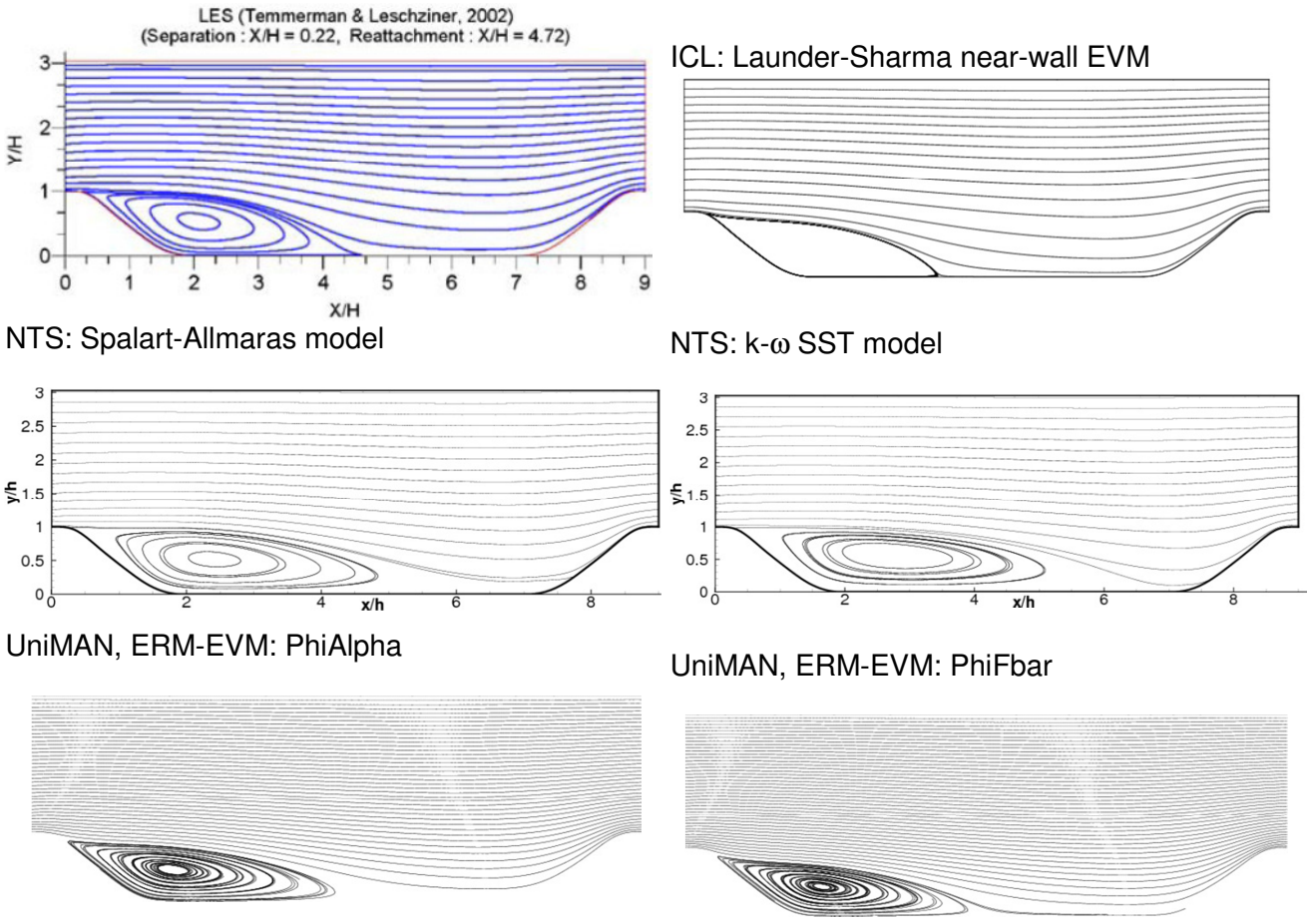

Figure 9: Re_H=10600, Eddy-viscosity model group – comparison of the time-averaged streamline patterns with the reference one (top left)

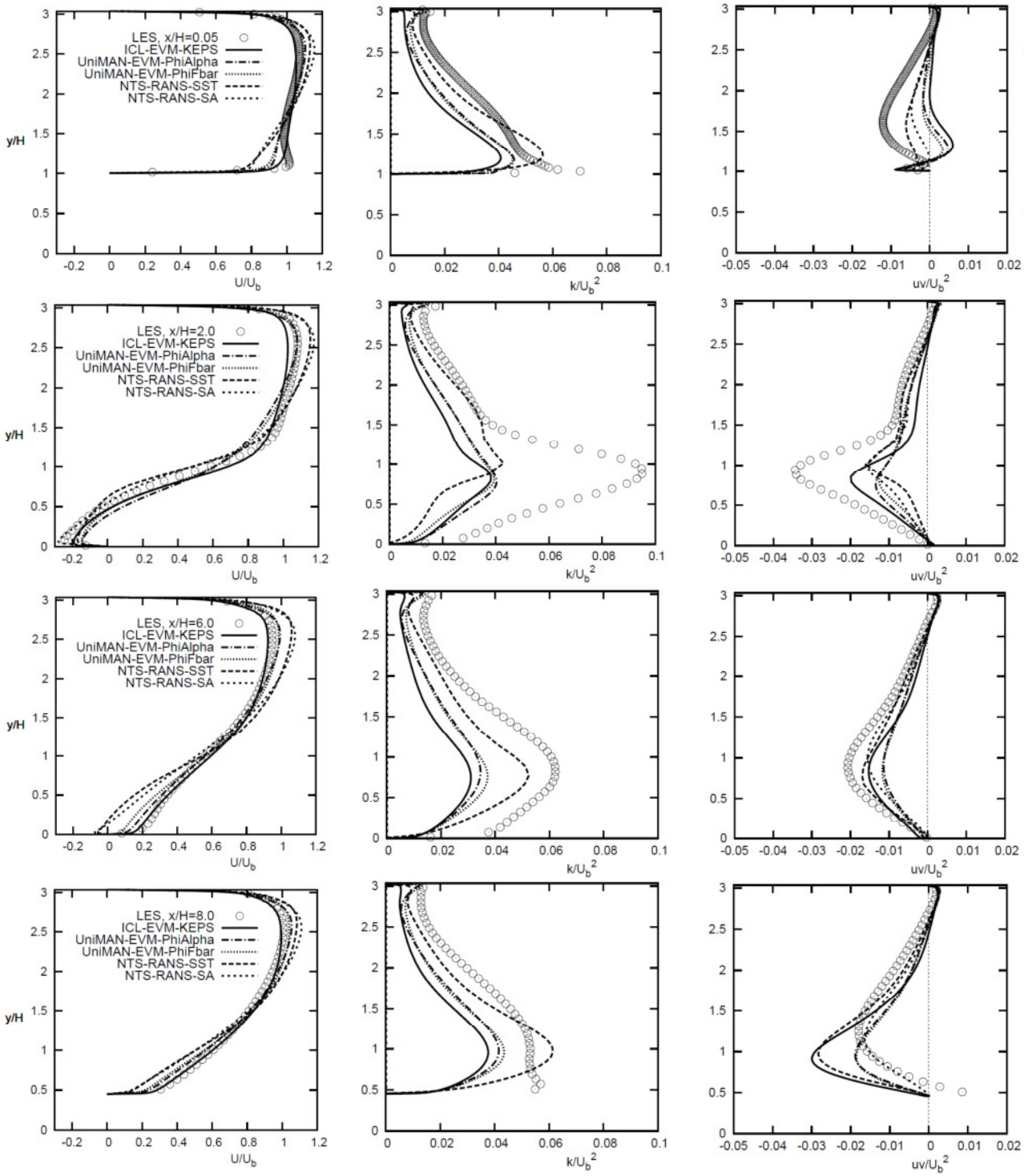

Figure 10: Re_H=10600, Eddy-viscosity model group – cross-plot comparison of axial velocity, turbulent kinetic energy and shear stress profiles at selected streamwise location *x/H=0.05*, *2.0*, *6.0* and *8.0*

Identifier	Partner	Model
ICL-RSM-LIN	ICL (Leschziner, Bentaleb)	Shima near-wall RSM model, 2D: 221x101 nodes
ICL-RSM-NLIN	ICL (Leschziner, Bentaleb)	Speziale et al. RSM model, near-wall extension due Chen, 2D: 161x161
FOI-DRSM	FOI (Wallin)	Wallin-Johansson near-wall DRSM + Hellsten ω-Eq., 2D: 161x161
FOI-EARSM-BSL	FOI (Wallin)	Wallin-Johansson near-wall EARSM + Menter's baseline ω-Eq., 2D: 161x161
FOI-EARSM-HWJ	FOI (Wallin)	Wallin-Johansson near-wall EARSM + Hellsten ω-Eq., 2D: 161x161
UniMAN-EBM	UniMAN (Billard, Revel)	EBM, near-wall DRSM (Manceau, Hanjalic) 2D: 120x172
TUD-DRSM	TUD (Maduta, Jakirlic)	Jakirlic-Hanjalic near-wall DRSM + ω_h-Eq., nlin, 2D, 160x160
TUD-DRSM-P_{SAS}	TUD (Maduta, Jakirlic)	Jakirlic-Hanjalic near-wall DRSM + ω_h–Eq. + Sl + (-P_{SAS}), nlin, 2D, 160x160
NUM-DRSM-SSG-ω	NUMECA (Temmerman, Hirsch)	SSG DRSM near-wall model coupled with ω-equation (Wilcox), 2D, 160x160

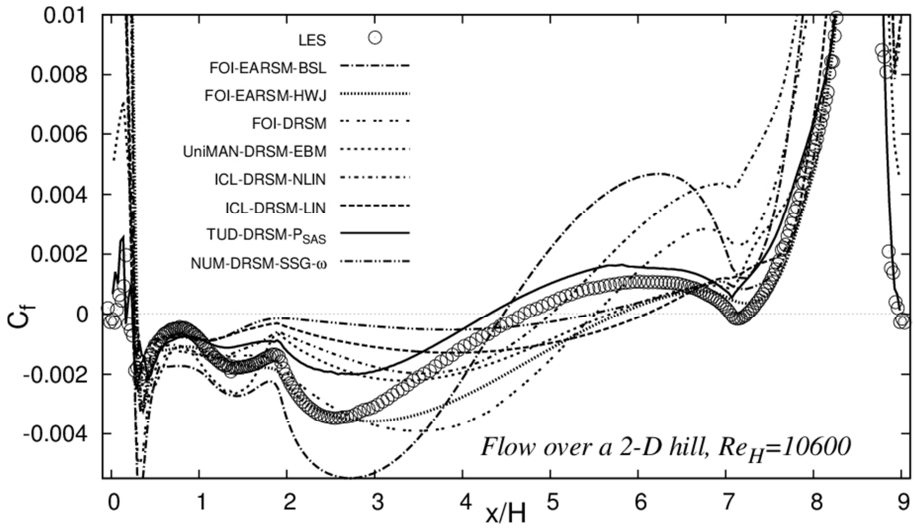

Figure 11: Re_H=10600, Reynolds stress model group – list of the contributors and the model used and friction factor

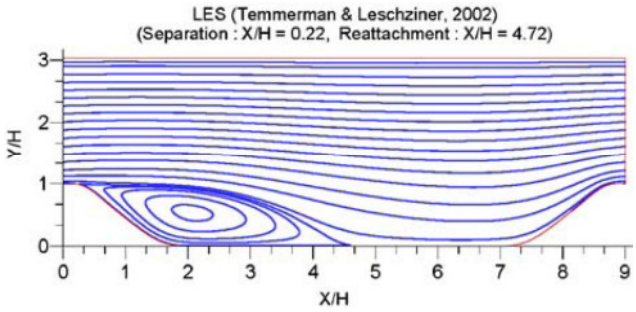

ICL: Speziale-Sarkar-Gatski RSM + Chen (near-wall extension)

NUM: SSG DRSM NW model + ω-Eq. (Wilcox)

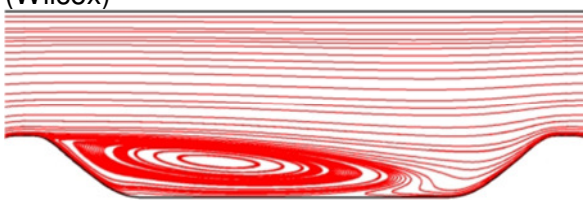

FOI: NW Wallin-Johansson DRSM + ω-Eq. (Hellsten)

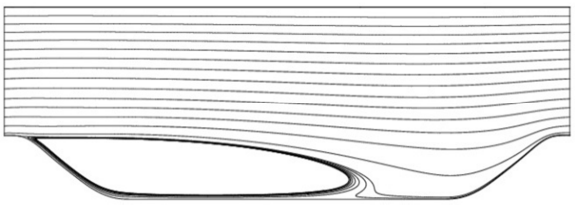

FOI: NW Wallin-Johansson EARSM + ω-Eq. (Hellsten)

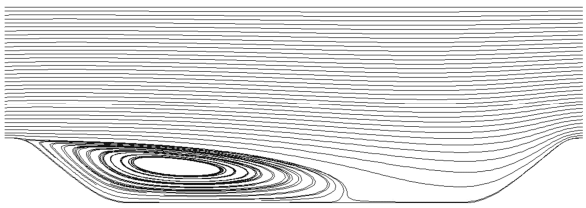

FOI: NW Wallin-Johansson EARSM + ω-Eq. (Menter bsl.)

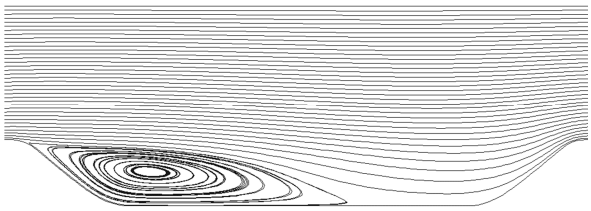

TUD: JH (non-linear) near-wall DRSM + ω_h–Eq.

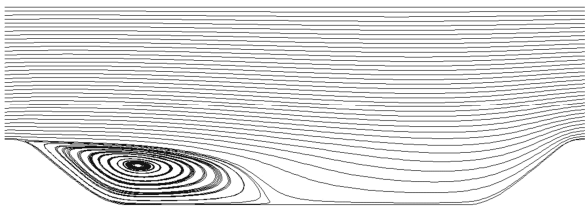

UniMan: EBM near-wall DRSM

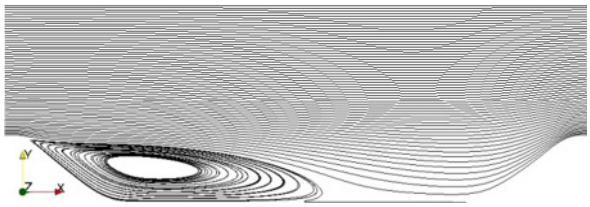

TUD: JH (non-linear) near-wall DRSM + ω_h–Eq. + Sl-Term + (-P_{SAS}) Term

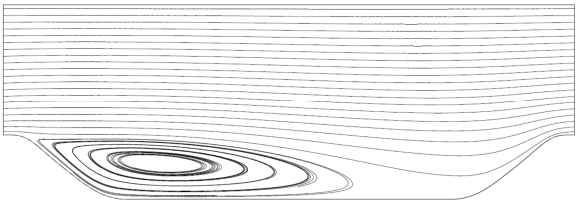

ICL: Shima near-wall RSM

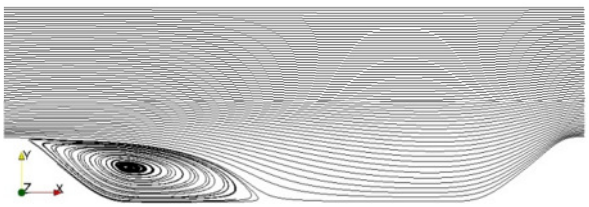

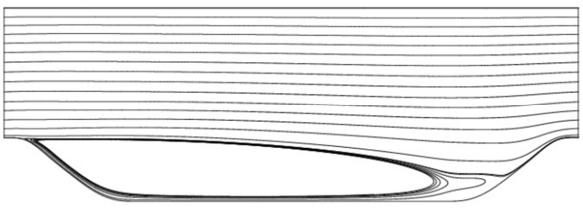

Figure 12: Re_H=10600, Reynolds stress model group – comparison of the time-averaged streamline patterns with the reference one (top left)

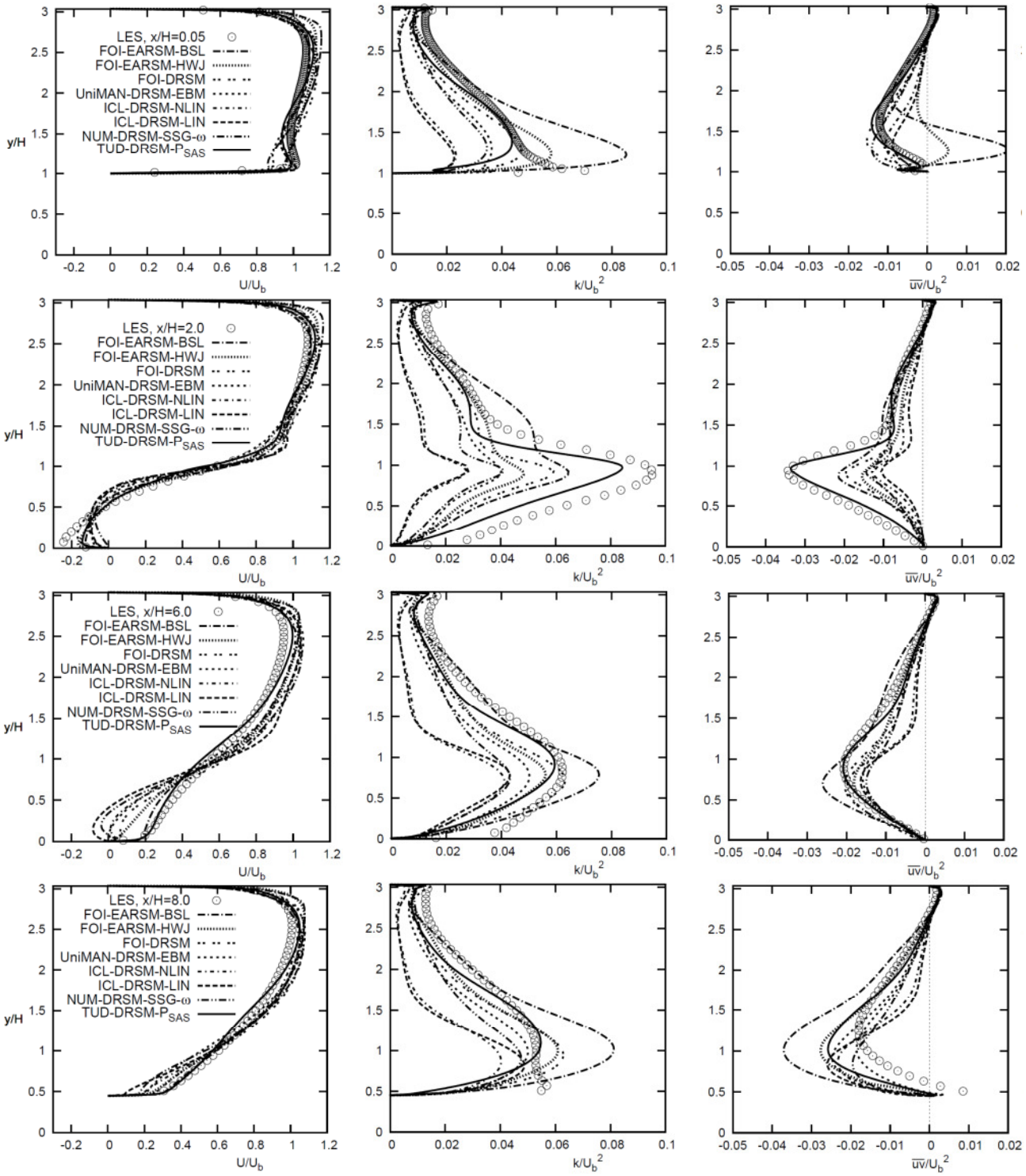

Figure 13: Re_H=10600, Reynolds stress model group – cross-plot comparison of axial velocity, turbulent kinetic energy and shear stress profiles at selected streamwise location *x/H=0.05*, *2.0*, *6.0* and *8.0*

Identifier	Partner	Model
NTS-SA-DDES	NTS (Strelets, Adamian)	DDES+SA NW model, 3D: 161x161x61 nodes
NTS-SA-IDDES	NTS (Strelets, Adamian)	IDDES+SA NW model, 3D: 161x161x61 nodes
NTS-SST-IDDES	NTS (Strelets, Adamian)	IDDES+SST NW model, 3D: 161x161x61 nodes
TUB-IDDES-SA-1	TUB (Fuchs, Mockett)	IDDES+SA, hybrid WBC, 3D: dt=0.015 160x160x120
TUB-IDDES-SA-2	TUB (Fuchs, Mockett)	IDDES+SA, hybrid WBC, 3D: dt=0.015, 160x78(equidistant)x120
TUB-IDDES-SA-3	TUB (Fuchs, Mockett)	IDDES+SA, hybrid WBC, 3D: dt=0.36 160x160x120
FOI-DES-SA	FOI (Peng)	DES + SA NW model, 3D, 160x80x32
FOI-kDES	FOI (Peng)	DES (1-Eq. Model based on k-Eq.), 3D, 160x80x64

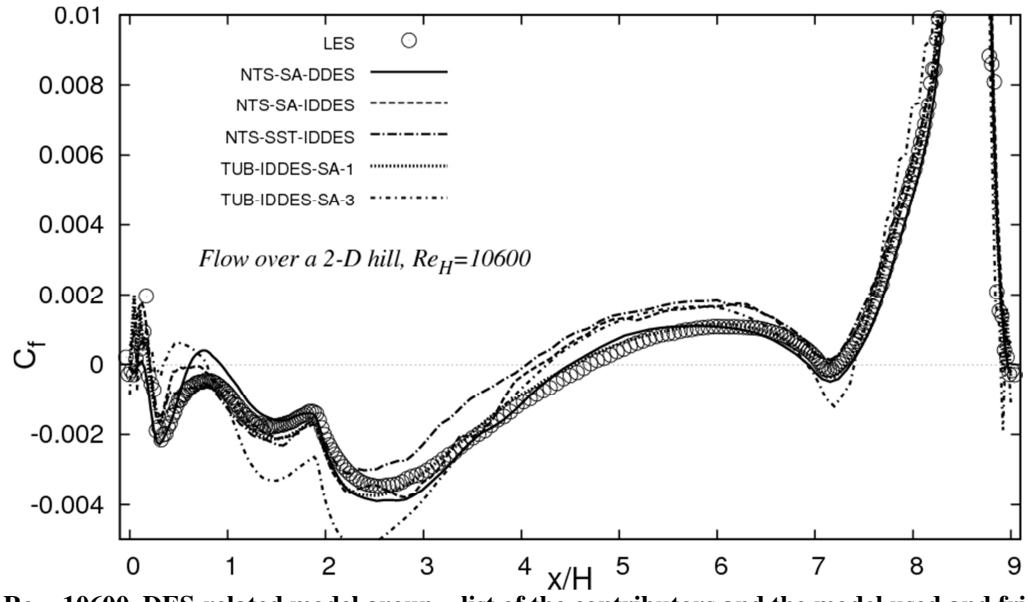

Figure 14: Re_H=10600, DES-related model group – list of the contributors and the model used and friction factor

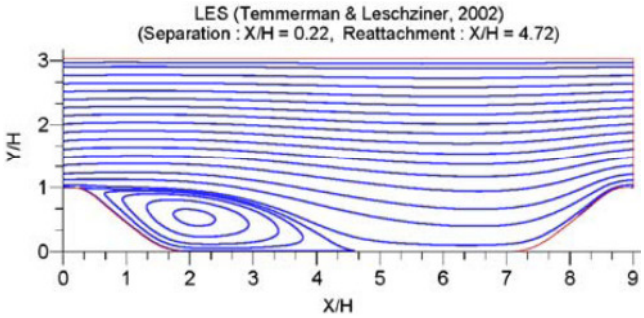

NTS: IDDES + SA (near-wall)

NTS: IDDES + SST (near-wall)

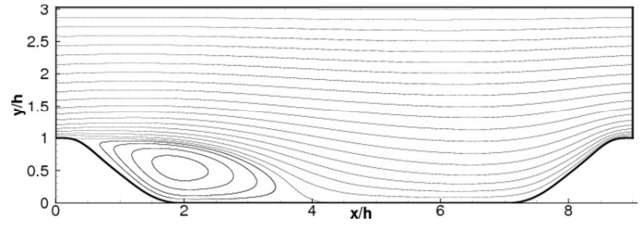

NTS: DDES + SA (near-wall)

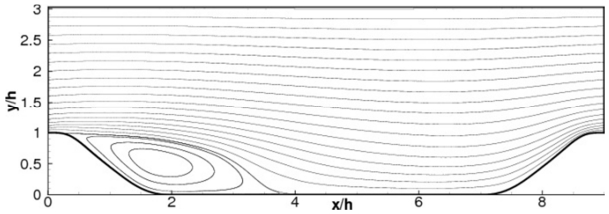

TUB: IDDES + SA 160x160x120, dt=0.015 (NW i.e. hybrid WBC)

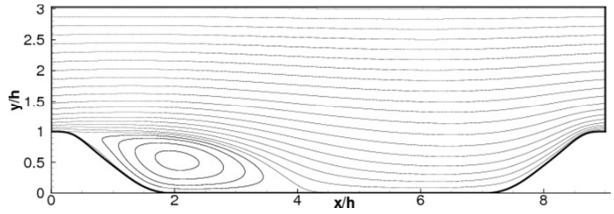

TUB: IDDES+SA 160x78(eq.)x120, dt=0.015 (hybrid WBC)

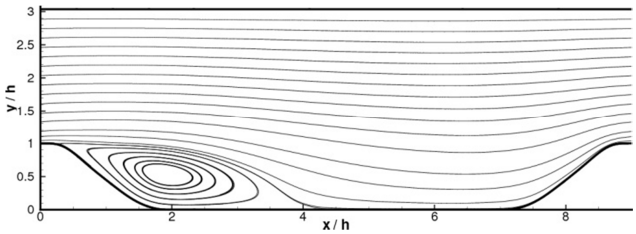

TUB: IDDES + SA 160x160x120, dt=0.36 (NW i.e. hybrid WBC)

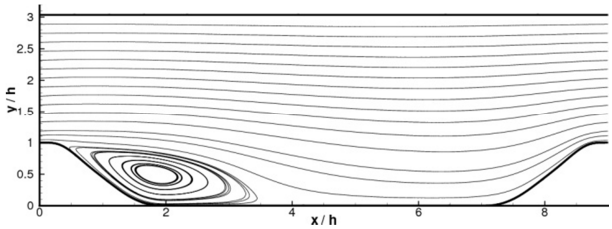

FOI: DES + SA NW model, 3D, 160x80x32

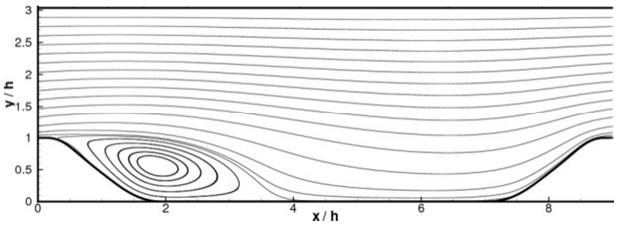

FOI: kDES (1-Eq. Model based on k-Eq.), 3D, 160x80x64

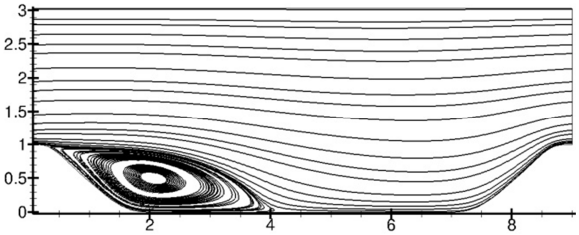

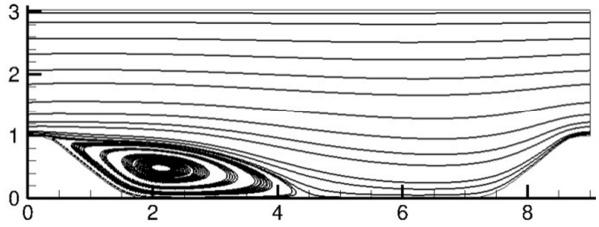

Figure 15: Re_H=10600, DES-related model group – comparison of the time-averaged streamline patterns with the reference one (top left)

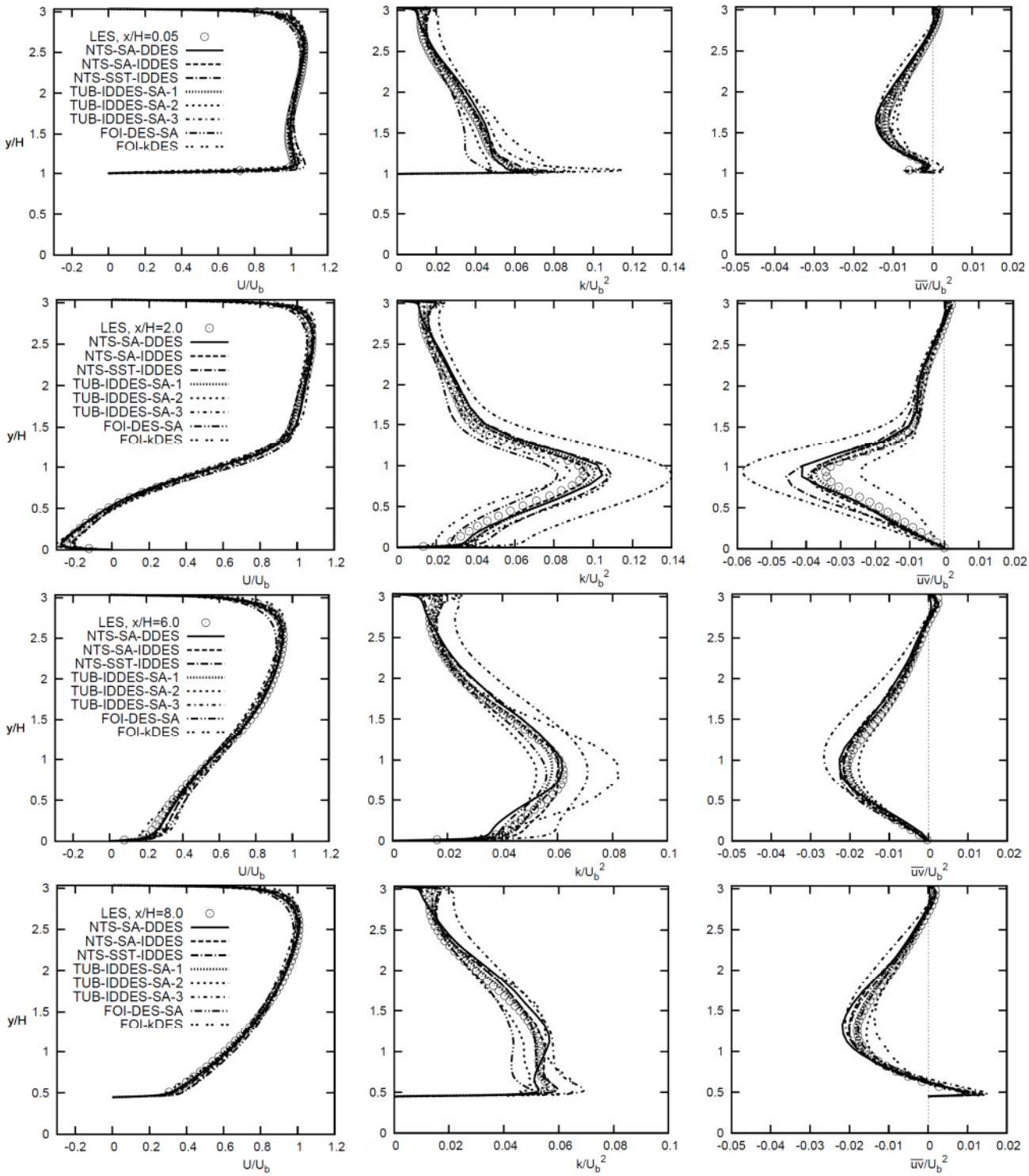

Figure 16: Re_H=10600, DES-related model group – cross-plot comparison of axial velocity, turbulent kinetic energy and shear stress profiles at selected streamwise location *x/H=0.05*, *2.0*, *6.0* and *8.0*

Identifier	Partner	Model
TUD-SAS-DRSM	TUD (Maduta, Jakirlic)	Near-wall DRSM (Jakirlic-Hanjalic) + ω^h-Eq. + Menter's et al. SAS term, 3D: 160x160x60
CHA-PANS-KEPS	CHA (Davidson)	PANS near-wall k-ε (Kondo, Abe, Nagano), 3D: 160x80x32
FOI-HYB0	FOI (Peng)	Seamless Hybrid RANS/LES based on 0-Eq. RANS model, 3D, 160x80x32
FOI-HYB0M	FOI (Peng)	Modified HYB0 model accounting for the energy back-scatter, 3D, 160x80x32
UniMan-HRLV2F	UniMan (Billard, Revel)	Hybrid RANS/LES based on phi-f ERM model (Uribe et al.)
ANS-SAS-SST	ANS (Schütze, Menter)	SAS version of the k-ω-SST model, 3D: 160x160x60

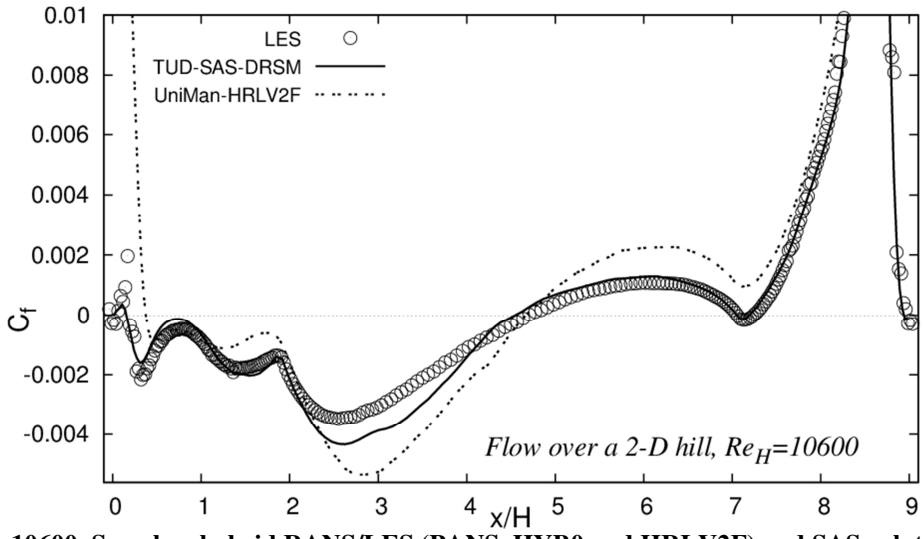

Figure 17: Re_H=10600, Seamless hybrid RANS/LES (PANS, HYB0 and HRLV2F) and SAS-related model group – list of the contributors and the model used and friction factor

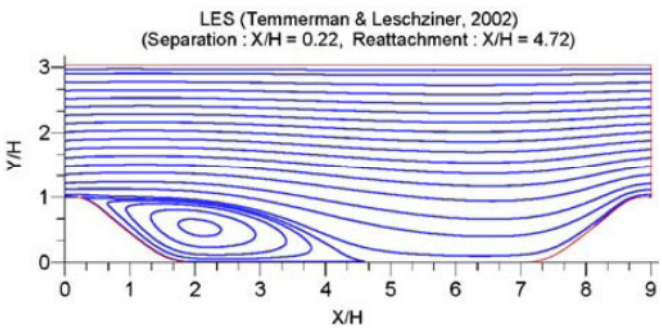

ANS: SAS version of the k-ω-SST model

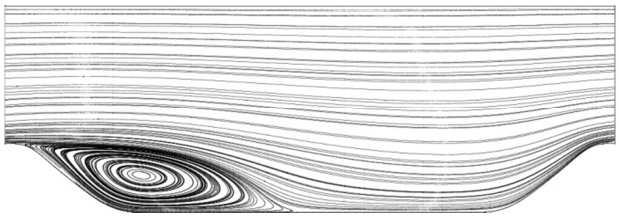

TUD: SAS-DRSM (JH non-linear near-wall DRSM + ω_h–Eq

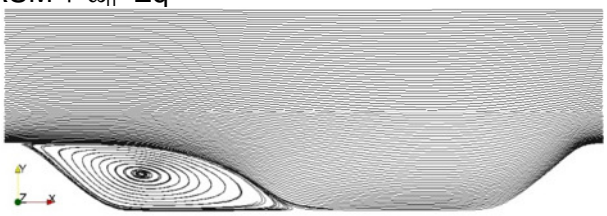

UniMan: Hybrid RANS/LES based on phi-f ERM model

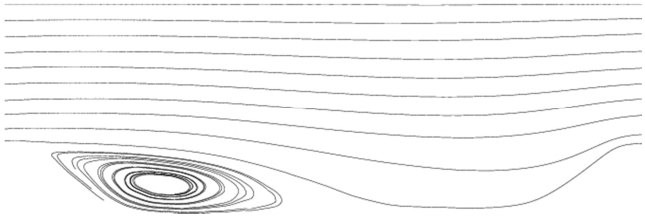

FOI: Seamless Hybrid RANS/LES based on 0-Eq. RANS model

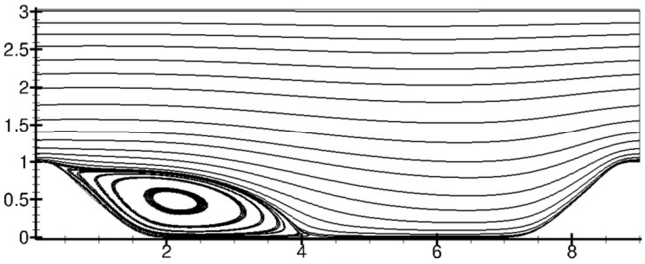

FOI: Modified HYB0 model accounting for the energy back-scatter

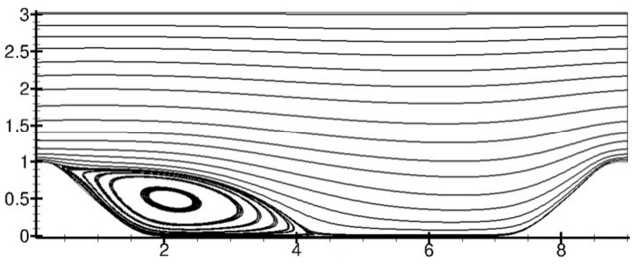

Figure 18: Re_H=10600, Seamless hybrid RANS/LES- (HRLV2F and HYB0) and SAS-related model group – comparison of the time-averaged streamline patterns with the reference one (top left)

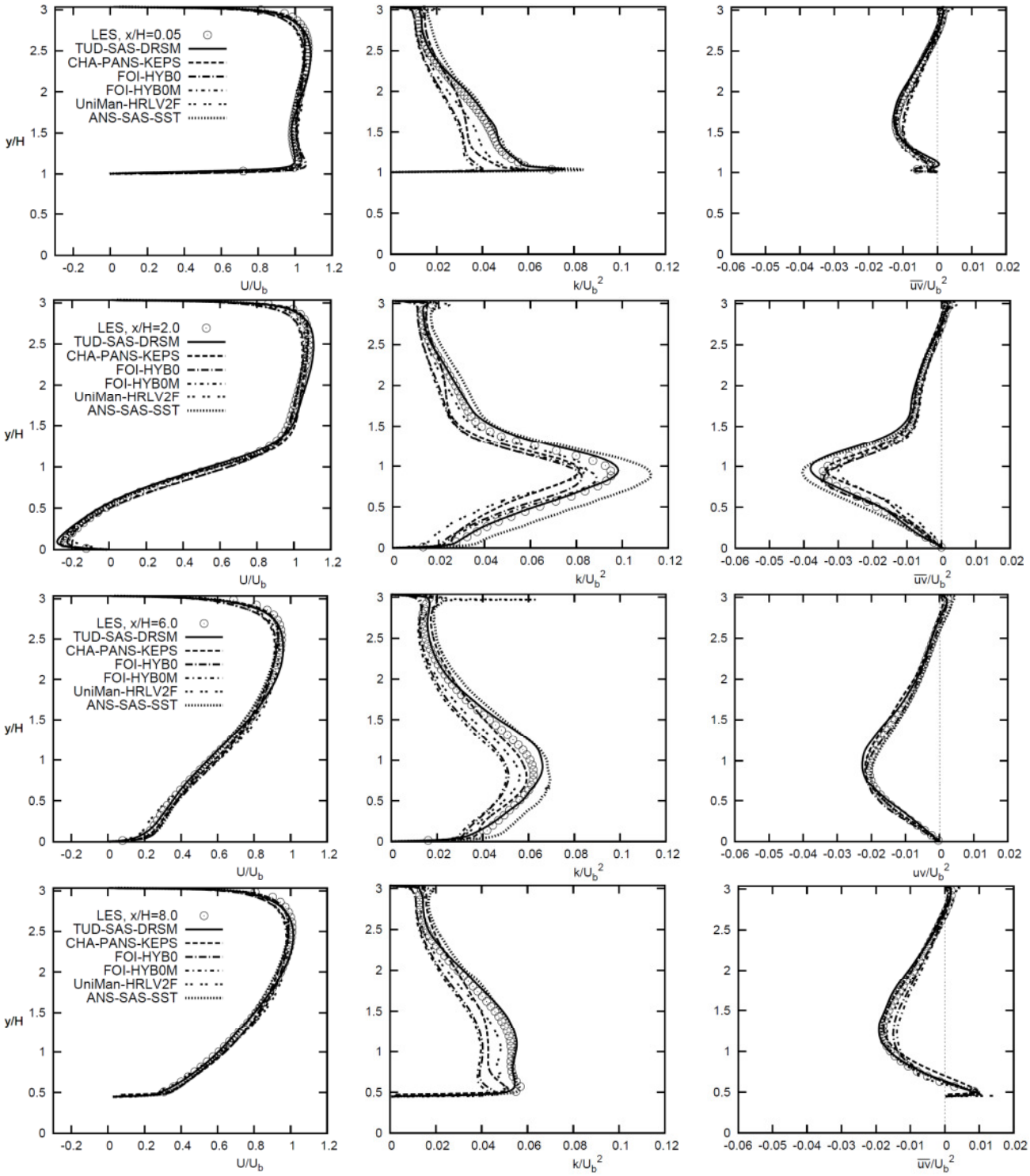

Figure 19: Re_H=10600, Seamless hybrid RANS/LES- (PANS, HYB0 and HRLV2F) and SAS-related model group – cross-plot comparison of axial velocity, turbulent kinetic energy and shear stress profiles at selected streamwise location *x/H=0.05*, *2.0*, *6.0* and *8.0*

Identifier	Partner	Model
TUD-DRSM-P_{SAS}	TUD (Maduta, Jakirlic)	Jakirlic-Hanjalic near-wall DRSM + ω_h–Eq. +Sl + (-P_{SAS}), nlin, 2D, 160x160
TUD-DRSM	TUD (Maduta, Jakirlic)	Jakirlic-Hanjalic near-wall DRSM + ω_h-Eq., nlin, 2D, 160x160
ICL-DRSM	ICL (Leschziner, Bentaleb)	Jakirlic-Hanjalic near-wall DRSM + ε-Eq., linear, 2D: 161x161
FOI-DRSM	FOI (Wallin)	Wallin-Johansson near-wall DRSM + Hellsten ω-Eq., 2D: 161x161
FOI-EARSM-BSL	FOI (Wallin)	Wallin-Johansson near-wall EARSM + Menter's baseline ω-Eq., 2D: 161x161
FOI-EARSM-HWJ	FOI (Wallin)	Wallin-Johansson near-wall EARSM + Hellsten ω-Eq., 2D: 161x161
NTS-RANS-SST	NTS (Strelets, Adamian)	Menter's k-ω SST near-wall model, 2D: 161x161
NUM-DRSM-SSG-ω	NUM (Temmerman, Hirsch)	SSG DRSM near-wall model coupled with ω-equation (Wilcox), 2D, 160x160

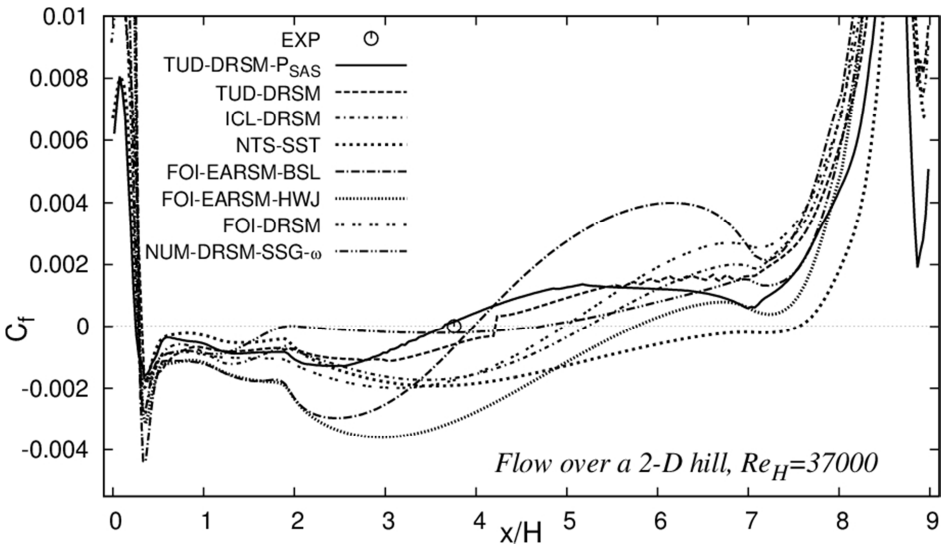

Figure 20: Re_H=37000, Reynolds stress model group and k-ω SST – list of the contributors and the model used and friction factor

ICL: Jakirlic-Hanjalic, linear, near-wall DRSM, ε-eq.

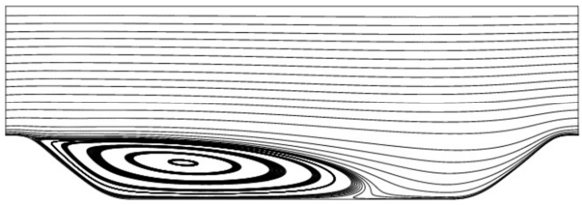

TUD: JH (non-linear) near-wall DRSM + ω_h–Eq. + Sl-Term + (-P_{SAS}) Term

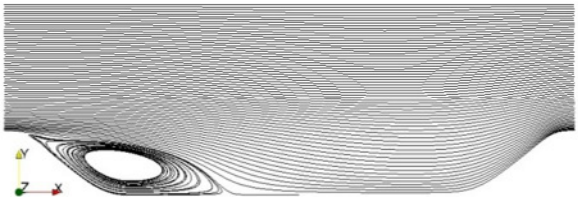

FOI: NW Wallin-Johansson EARSM + ω-Eq. (Hellsten)

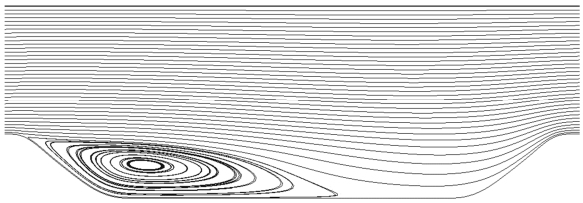

NTS: k-ω SST model

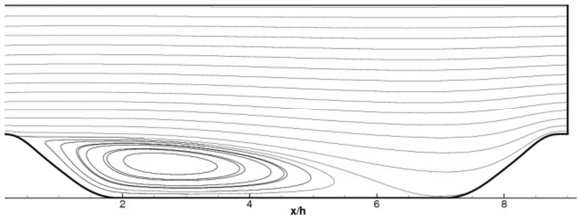

TUD: JH (non-linear) near-wall DRSM + ω_h–Eq.

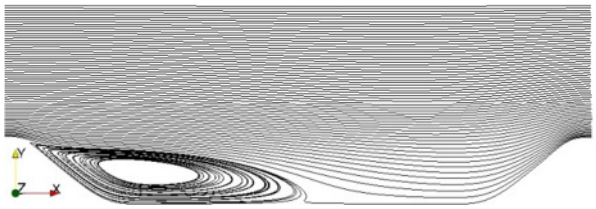

FOI: NW Wallin-Johansson DRSM + ω-Eq. (Hellsten)

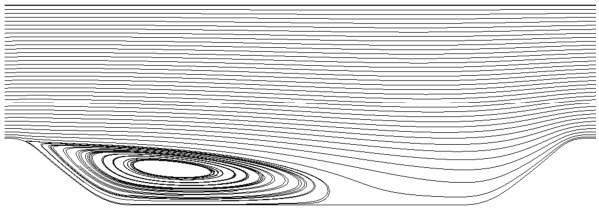

FOI: NW Wallin-Johansson EARSM + ω-Eq. (Menter bsl.)

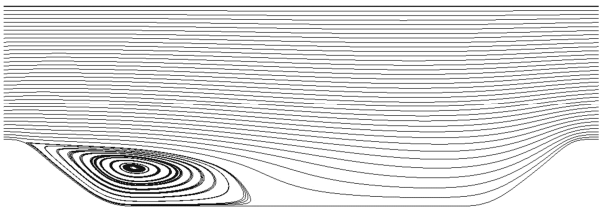

NUM: DRSM-SSG + ω - Eq. (Wilcox)

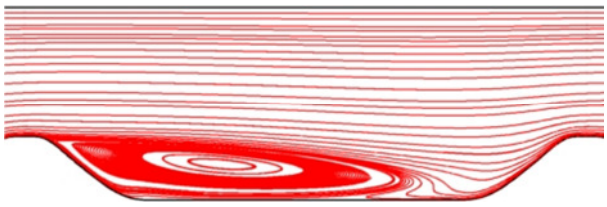

Figure 21: Re_H=37000, Reynolds stress model group and k-ω SST – mutual comparison of the time-averaged streamline patterns

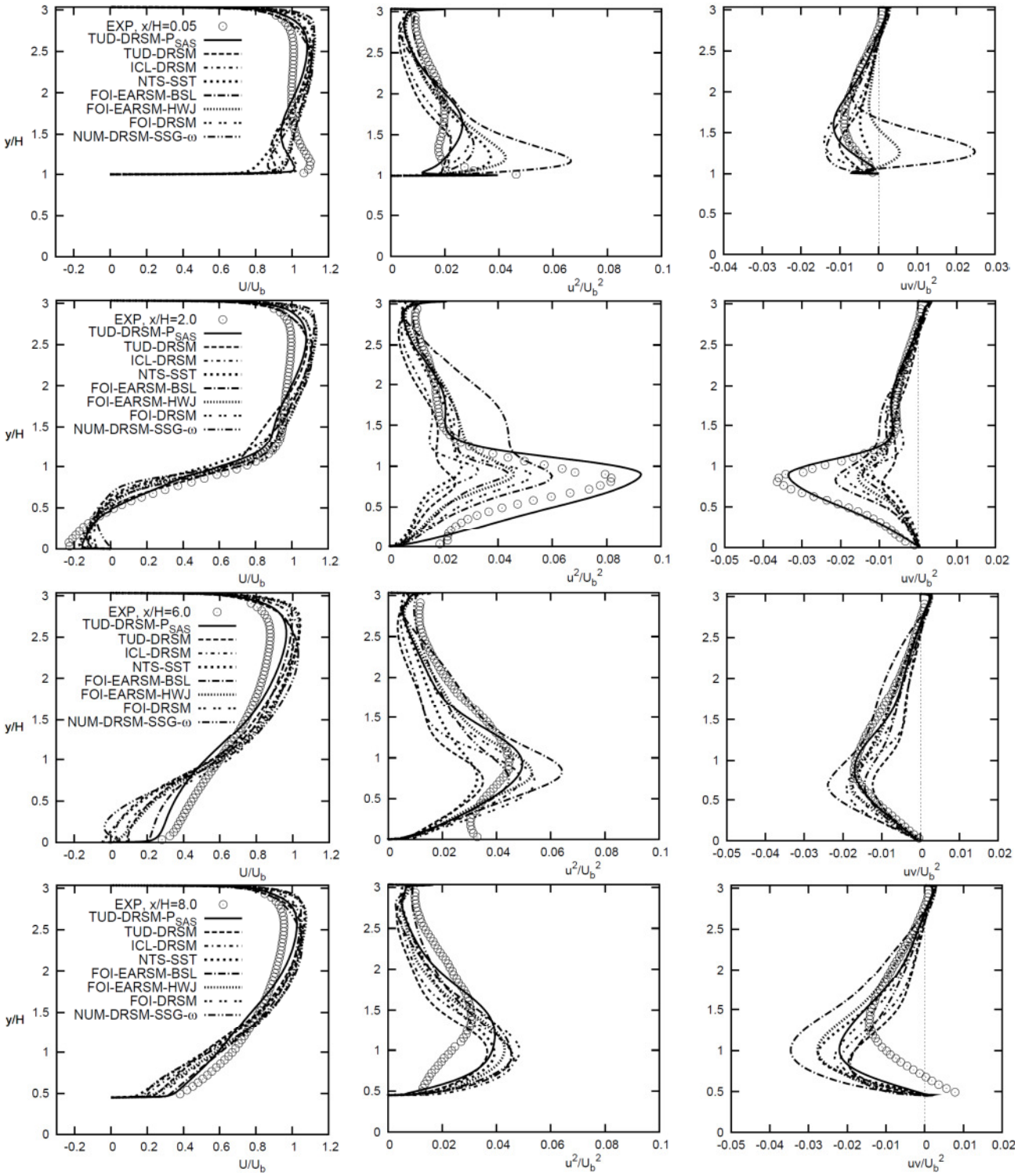

Figure 22: Re_H=37000, Reynolds stress model group and k-ω SST – cross-plot comparison of axial velocity, streamwise and shear stress component profiles at selected streamwise location *x/H=0.05*, *2.0*, *6.0* and *8.0*

Identifier	Partner	Model
NTS-SST-IDDES	NTS (Strelets, Adamian)	IDDES+SA NW model, 3D: 161x181x61 nodes
TUB-IDDES-SA-1	TUB (Fuchs, Mockett)	IDDES+SA, hybrid WBC, 3D: dt=0.015 160x160x120
TUB-IDDES-SA-2	TUB (Fuchs, Mockett)	IDDES+SA, hybrid WBC, 3D: dt=0.015, 160x78(equidistant)x120
TUD-SAS-DRSM	TUD (Maduta, Jakirlic)	Near-wall DRSM (Jakirlic-Hanjalic) + ω^h-Eq. + Menter's et al. SAS term, 3D: 160x160x60
CHA-PANS-KEPS	CHA (Davidson)	PANS near-wall k-ε (Kondo, Abe, Nagano), 3D: 160x80x32
FOI-HYB0	FOI (Peng)	Seamless Hybrid RANS/LES based on 0-Eq. RANS model, 3D, 160x80x32
ANS-SAS-SST	ANS (Schütze, Menter)	SAS version of the k-ω-SST model, 3D: 160x160x60
IMFT-DES-SA	IMFT (Gual-Skopek, Braza)	DES+SA, NW model, 160x160x60 CVs, block(32)-structured hexa-mesh
IMFT-DDES-SST	IMFT (Gual-Skopek, Braza)	DDES+SST, NW model, 160x160x60 CVs, block(32)-structured hexa-mesh

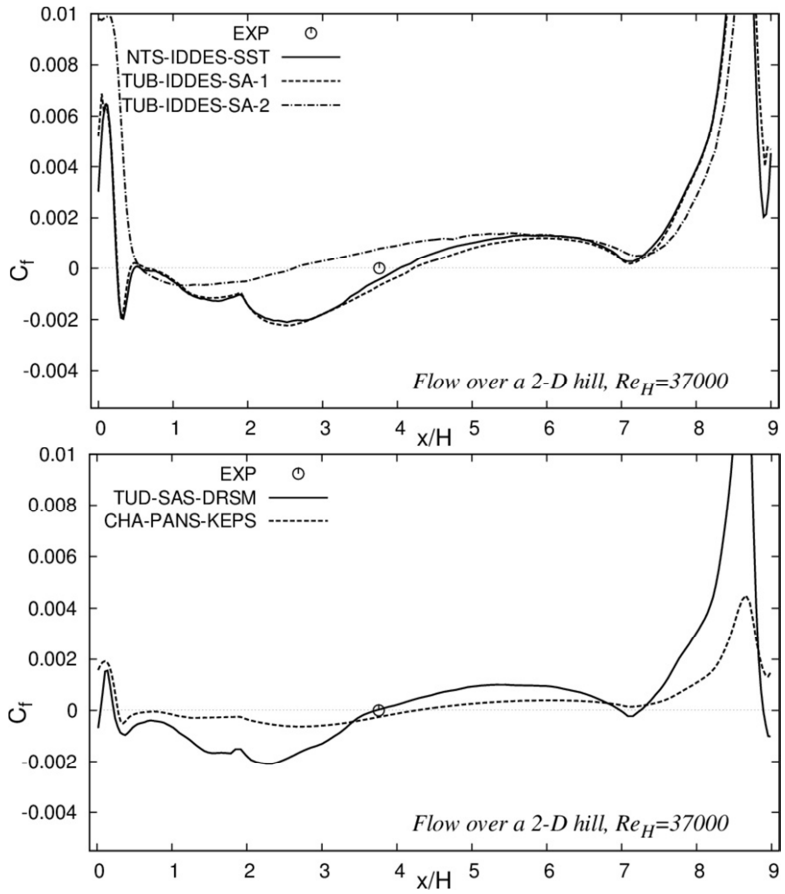

Figure 23: Re_H=37000, DES-, PANS-, SAS- and other hybrid LES/RANS-related model group – list of the contributors and the model used and friction factor

NTS: IDDES + SST (near-wall)

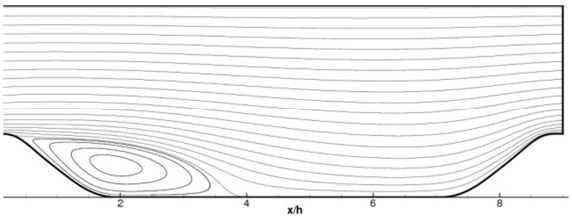

TUD: SAS-DRSM (JH non-linear near-wall DRSM + ω_h–Eq.)

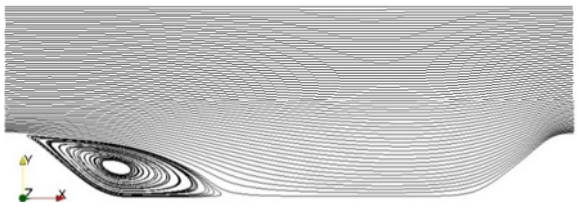

TUB: IDDES + SA 160x160x120, dt=0.015 (NW i.e. hybrid WBC)

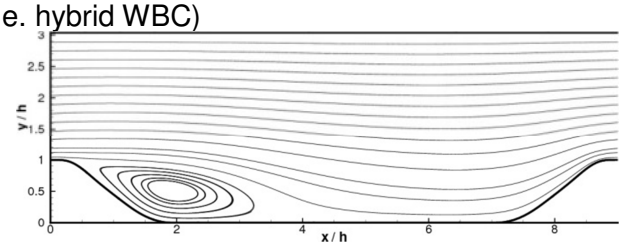

TUB: IDDESSA 160x78(eq.)x120, dt=0.015 (hybrid WBC)

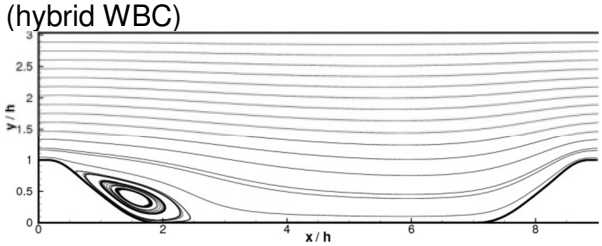

FOI: HYB0 - Seamless Hybrid RANS/LES based on 0-Eq. RANS model

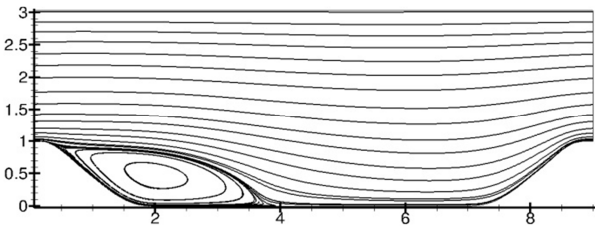

ANS: SAS version of the k-ω-SST model

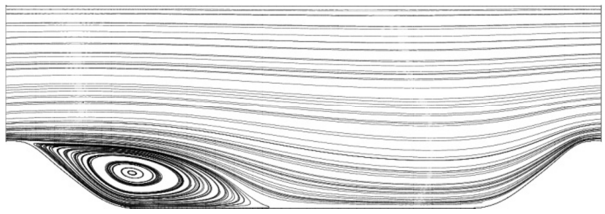

IMFT: DES+SA, NW model, 160x160x60 CVs, block(32)-structured hexa-mesh

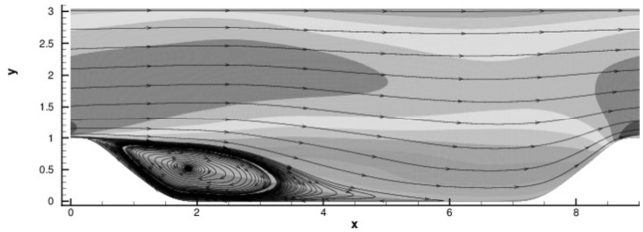

IMFT: DDES+SST, NW model, 160x160x60 CVs, block(32)-structured hexa-mesh

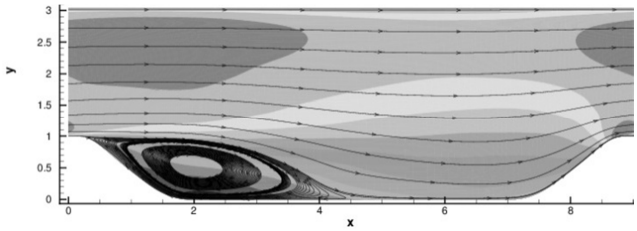

Figure 24: Re_H=37000, DES-, PANS- and SAS-related model group – mutual comparison of the time-averaged streamline patterns

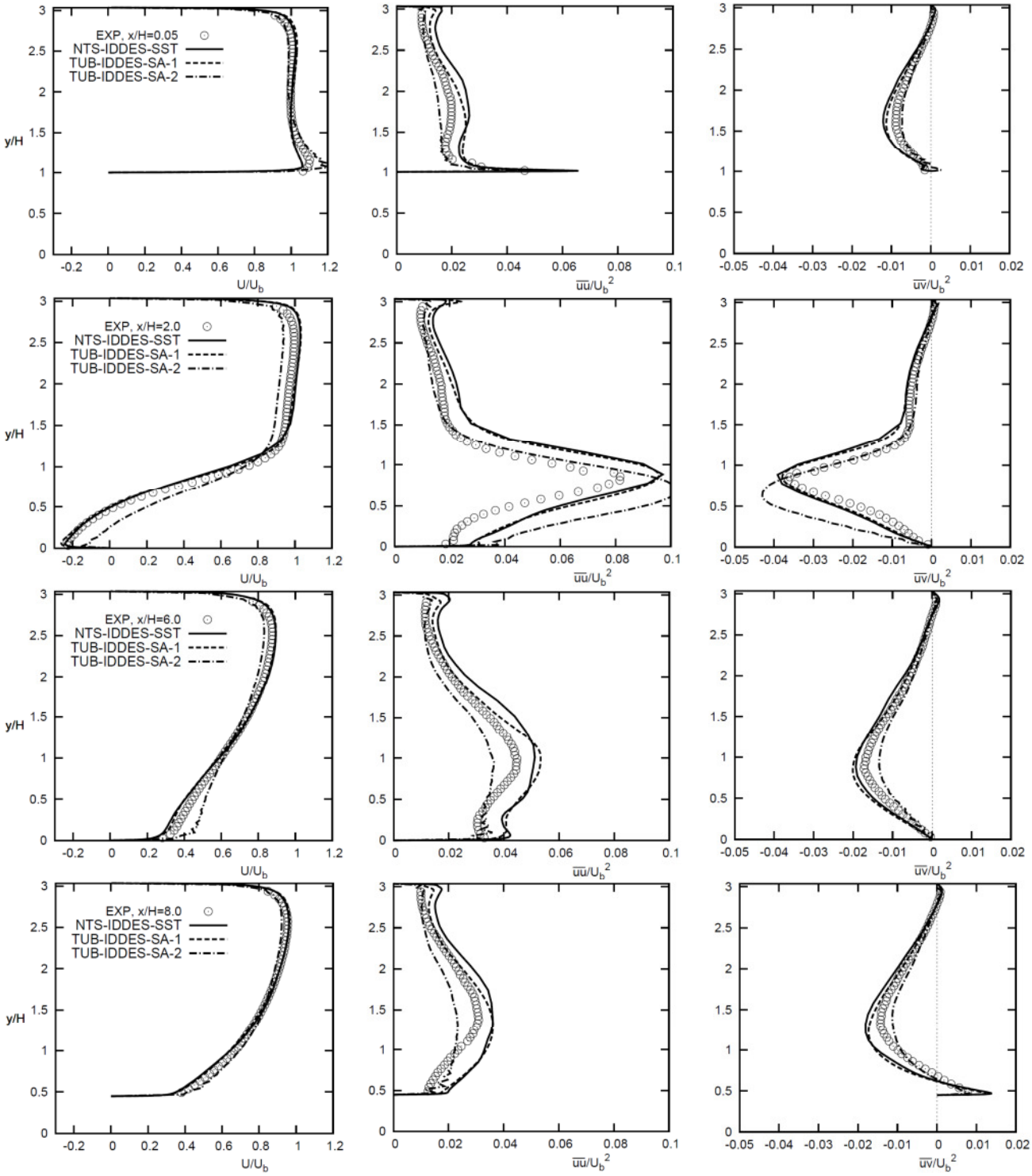

Figure 25-1: Re_H=37000, DES-related model group – cross-plot comparison of axial velocity, streamwise and shear stress component profiles at selected streamwise location *x/H=0.05*, *2.0*, *6.0* and *8.0*

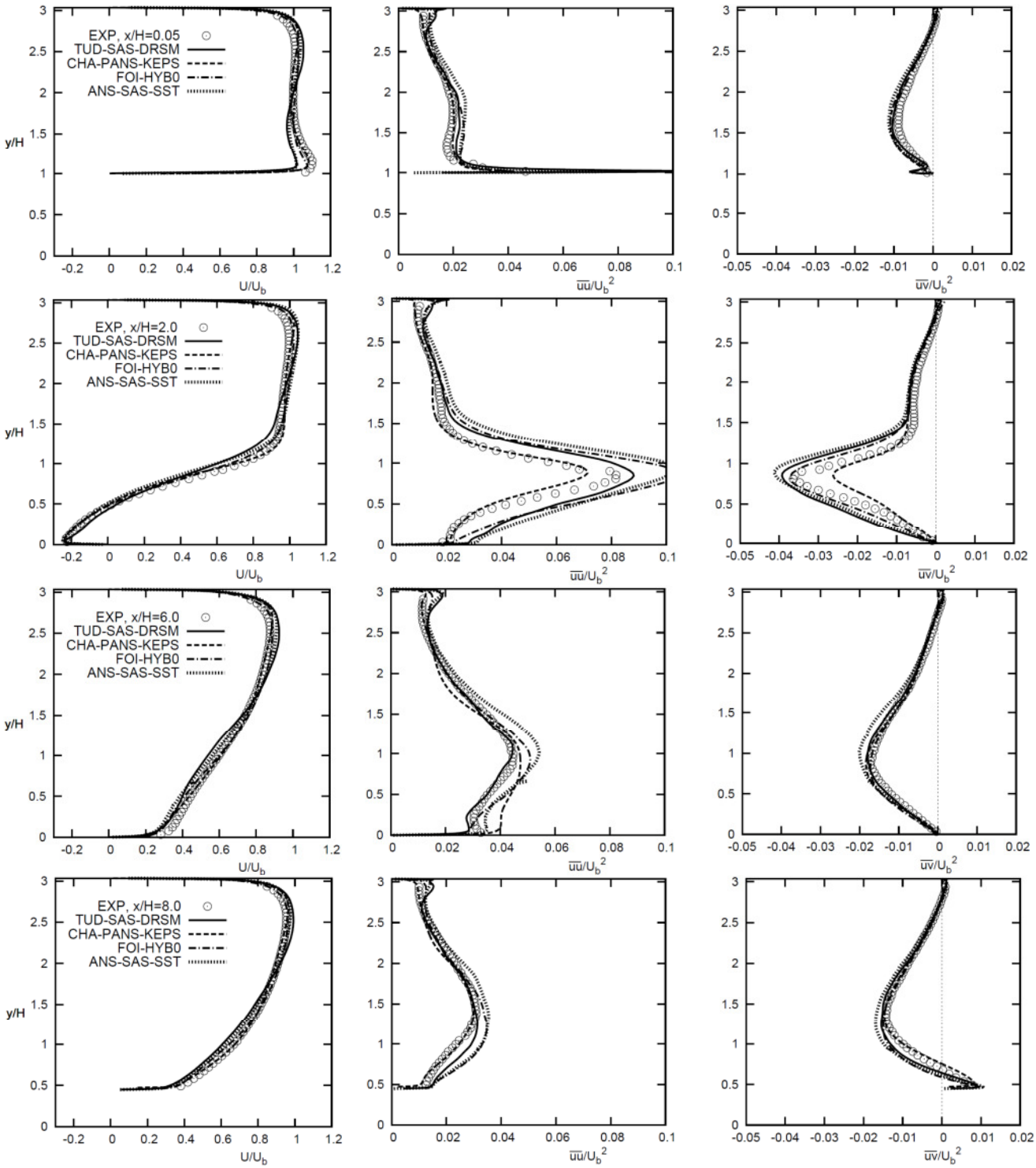

Figure 26-2: Re_H=37000, PANS-, SAS- and Hybrid LES/RANS-related model group – cross-plot comparison of axial velocity, streamwise and shear stress component profiles at selected streamwise location *x/H=0.05*, *2.0*, *6.0* and *8.0*

References

1) Billard, F., Laurence, D. and Uribe, J. (2010): An improved dissipation rate equation for the v2f model to account for turbulent transport mechanism in a boundary layer. 8th Interntational ERCOFTAC Symosium. on Engineering Turbulence Modelling and Measurements (ETMM8), Marseille, France, June 9-11.
2) Breuer, M. (2005): New reference data for the hill flow test case. http://www.hy.bv.tum.de/DFG-CNRS/
3) Breuer, M., Peller, N., Rapp, Ch. and Manhart, M. (2009): Flow over periodic hills – Numerical and experimental study in a wide range of Reynolds numbers. *Computers and Fluids*, Vol. 38, pp. 433-457
4) Fröhlich, J., Mellen, C.P., Rodi, W., Temmerman, L. and Leschziner, M.A. (2005): Highly resolved large-eddy simulation of separated flow in a channel with streamwise periodic constrictions. *Journal of Fluid Mechanics.*, Vol. 526, pp. 19-66
5) Hellsten, A. (2004): New advanced k-ω turbulence model for high-lift aerodynamics. AIAA Paper 2004-1120, 42nd Aerospace Sciences Meeting and Exhibit, Reno, Nevada.
6) Jarrin, N., Prosser, R., Uribe, J., Benhamadouche, S., Laurence, D. (2009): Reconstruction of Turbulent Fluctuations for Hybrid RANS-LES simulations using a synthetic Eddy Method, *Int. Journal of Heat and Fluid Flow*, Vol. **30**, pp. 435-442.
7) Jakirlić, S. and Hanjalić K. (2002): A new approach to modelling near-wall turbulence energy and stress dissipation. *J. Fluid Mech.* Vol. **439**, pp. 139-166
8) Jakirlić, S., Jester-Zürker, R. and Tropea, C. (2002): Report on 9th ERCOFTAC/IAHR/COST Workshop on Refined Turbulence Modelling. October, 9-10, 2001, Darmstadt University of Technology, *ERCOFTAC Bulletin*, No. 55, pp. 36-43
9) Jakirlić, S., Kniesner, B. and Kadavelil, G. (2011): On interface issues in LES/RANS coupling strategies: a method for turbulence forcing. *JSME Journal of Fluid Science and Technology* , Vol. **6**, No. **1**, pp. 56-72
10) Launder, B.E., and Sharma, B.I. (1974): Application of the Energy-Dissipation Model of Turbulence to the Calculation of Flow Near a Spinning Disc. *Letters in Heat and Mass Transfer*, Vol. 1, pp. 131-138
11) Laurence, D. Uribe, J. C. and Utyuzhnikov, S. V. (2004): A robust formulation of the v2f model, *Flow Turbulence and Combustion*, Vol. 73, pp. 169-185.
12) Leschziner, M.A. (2002): Test Case 9.2: The flow in a channel with periodic 'hills' on one wall. Proceedings of the 10th joint ERCOFTAC (SIG 15)/IAHR/QNET-CFD Workshop on refined Turbulence Modelling, University of Poitiers, France, October 10-11
13) Ma, J.-M., Peng, S.-H., Davidison, L. and Wang, F. (2011): A low Reynolds number variant of partially-averaged Navier-Stokes model for turbulence. *Int. J. Heat and Fluid Flow*, Vol. 32(3), pp. 652-669
14) Maduta, R. and Jakirlić, S. (2011): An eddy-resolving Reynolds stress transport model for unsteady flow computations. In "Advances in Hybrid RANS-LES Modelling 4". *Notes on Numerical Fluid Mechanics and Multidisciplinary Design*, Vol. 117, S. Fu, W. Haase, S.-H. Peng and D. Schwamborn (Eds.), pp. 77-89, Springer Verlag (ISBN 978-3-642-31817-7)
15) Manceau, R. (2003): Report on 10th ERCOFTAC (SIG-15)/IAHR/QNET-CFD Workshop on Refined Turbulence Modelling. October 10-11, 2002, University of Poitiers, *ERCOFTAC Bulletin*, No. **57**
16) Manceau, R. and Hanjalic, K. (2002): The elliptic blending model: a new near-wall Reynolds-stress closure. *Physics of Fluids*, Vol. **14**, No. **2**, pp. 744-754
17) Mellen, C. P., Froehlich, J. and Rodi, W. (2000): Large eddy simulation of the flow over periodic hills, Proceedings IMACS World Congress (ed. M. Deville and R. Owens), Lausanne
18) Menter, F.R. (1994): Two-equation eddy-viscosity turbulence models for engineering applications, *AIAA Journal*, Vol. 32, No. 8, pp. 1598-1605.

19) Menter, F. R., Garbaruk, A.V. and Egorov, Y. (2009): Explicit Algebraic Reynolds Stress Models for Anisotropic Wall-Bounded Flows, Proceedings of 3rd European Conference for Aero-Space Sciences (EUCASS), July 6-9th, Versailles.

20) Menter, F.R., Kuntz, M. and Bender, R. (2003): A scale adaptive simulation model for turbulent flow predictions. AIAA Paper 2003-0767.

21) Menter, F.R. and Egorov, Y. (2010): The scale-adaptive simulation method for unsteady turbulent flow predictions. Part I: theory and model description. *Flow Turbulence and Combustion*, Vol. **85**, pp. 113-138

22) Peng, S.-H. (2005): Hybrid RANS-LES modelling based on zero- and one-equation models for turbulent flow simulation. In Proceedings of *4th International Symposium on Turbulence and Shear Flow Phenomena*, Vol. **3**, pp. 1159-1164

23) Peng, S.-H. (2006): Algebraic hybrid RANS-LES modelling applied to incompressible and compressible turbulent flows. AIAA Paper 2006-3910. San Francisco,

24) Peng, S.-H. and Leicher, S. (2008): DES and hybrid RANS-LES modelling of unsteady pressure oscillations and flow features in a rectangular cavity. In Advances in Hybrid RANS-LES Modelling, (Eds) S.-H. Peng and W. Haase. Notes on Numerical Fluid Mechanics and Multidisplinary Design, Vol. **97**, pp.132-141

25) Rapp C. (2008): Experimentelle Untersuchung der turbulenten Strömung über periodische Hügel. PhD Thesis, Technical University Munich, Germany

26) Rapp, C. and Manhart, M. (2011): Flow over periodic hills: an experimental study. *Experiments in Fluids*, Vol. **51**, pp. 247-269

27) Shima, N. (1993): Prediction of Turbulent Boundary Layers With a Second-Moment Closure: Part I - Effects of Periodic Pressure Gradient, Wall Transpiration and Free-Stream Turbulence. *ASME J. of Fluids Engng.*, Vol. **115**, pp. 56-63

28) Spalart, P.R. (2001): Young-person's guide to Detached-Eddy Simulation Grids. NASA-CR 211032.

29) Spalart, P.R. and Allmaras, S.R. (1994) A one-equation turbulence model for aerodynamic flows. *La Recherche Aerospatiale*, Vol. **1**, pp. 5-21 (see also AIAA Paper 92-0439)

30) Spalart, P.R. (2009): Detached-Eddy Simulation. *Annual Review of Fluid Mechanics*, Vol. **41**, pp. 181-202.

31) Speziale, C.G., Sarkar, S. and Gatski, T.B. (1991): Modelling the Pressure-Strain Correlation of Turbulence: an Invariant Dynamical Systems Approach. *J. Fluid Mech.*, Vol. **227**, pp. 245-272

32) Temmerman, L. and Leschziner, M.A. (2001): Large Eddy Simulation of separated flow in a streamwise periodic channel construction, Second International. Symposium on Turbulence and Shear Flow Phenomena, Stockholm, June 27-29

33) Uribe, J., Jarrin, N., Prosser, R. and Laurence, D. (2010): Development of a Two-velocities Hybrid RANS-LES Model and its Application to a Trailing Edge Flow, *Flow Turbulence and Combustion*, Vol. **85**, pp. 181 – 197.

34) Wallin, S. and Johansson, A.V., (2000) An explicit algebraic Reynolds stress model for incompressible and compressible turbulent flows, *Journal of Fluid Mechanics*, Vol. **403**, pp. 89–132

35) Wilcox, D.C. (1988) Reassessment of the scale-determining equation for advanced turbulence models, *AIAA Journal*, Vol. **33**,(11), pp. 1299-1310